# The importance of ice shelf melt rate distributions in modelling of Antarctic ice loss

| | |
|---|---|
| Journal: | *Annals of Glaciology* |
| Manuscript ID | AOG-100-0588 |
| Manuscript Type: | Article |
| Date Submitted by the Author: | 03-Sep-2026 |
| Complete List of Authors: | Barnes, Jowan; Northumbria University,<br>Gudmundsson, Gudmundur Hilmar; Northumbria University - City Campus,<br>Timmermann, Ralph; Alfred Wegener Institute for Marine and Polar Research |
| Keywords: | Ice/ocean interactions, Melt - basal, Ice-sheet modelling, Antarctic glaciology |
| Abstract: | Ocean-induced basal melting of ice shelves is a major cause of Antarctic ice loss. It is well known that the magnitude of this melt is an important factor to consider when modelling the future evolution of the ice sheet, and values of total melt volume or mean melt rates are often quoted for ice shelves. The finer detail of the distribution of this melt is usually given less attention. Here we make the argument for using coupled modelling frameworks such as Úa-FESOM, which employs unstructured triangular meshes in both the ice sheet and ocean components, providing added flexibility in resolving critical areas of ocean circulation and ice flow. We validate our model outputs by assessing correlation with Antarctic-wide observationally derived ice shelf basal melt rates, and a simple depth-based parameterisation of the type used in standalone ice sheet modelling. We show that the distribution of melt - independently of total melt volume - can significantly affect modelled ice flow, and we investigate the role of mesh resolutions in both components. Our results demonstrate the need for setups like Úa-FESOM, showing differences of 10% in the first year of ice sheet responses due to differing melt distributions and model resolutions. |
| | |

Annals of Glaciology 68(1) 2026 [preprint] 1

# The importance of ice shelf melt rate distributions in modelling of Antarctic ice loss

Jowan M. BARNES[1], G. Hilmar GUDMUNDSSON[1], Ralph TIMMERMANN[2]

[1]*School of Geography and Natural Sciences, Northumbria University, Newcastle upon Tyne, United Kingdom*

[2]*Physical Oceanography of Polar Seas, Alfred Wegener Institute, Bremerhaven, Germany*

*Correspondence: Jowan Barnes <jowan.barnes@northumbria.ac.uk>*



**ABSTRACT. Ocean-induced basal melting of ice shelves is a major cause of Antarctic ice loss. It is well known that the magnitude of this melt is an important factor to consider when modelling the future evolution of the ice sheet, and values of total melt volume or mean melt rates are often quoted for ice shelves. The finer detail of the distribution of this melt is usually given less attention. Here we make the argument for using coupled modelling frameworks such as Úa-FESOM, which employs unstructured triangular meshes in both the ice sheet and ocean components, providing added flexibility in resolving critical areas of ocean circulation and ice flow. We validate our model outputs by assessing correlation with Antarctic-wide observationally derived ice shelf basal melt rates, and a simple depth-based parameterisation of the type used in standalone ice sheet modelling. We show that the distribution of melt – independently of total melt volume – can significantly affect modelled ice flow, and we investigate the role of mesh resolutions in both components. Our results demonstrate the need for setups like Úa-FESOM, showing differences of 10% in the first year of ice sheet responses due to differing melt distributions and model resolutions.**

# INTRODUCTION

Basal melting driven by interaction with the ocean is the primary cause of mass loss on two thirds of Antarctica's ice shelves (Davison and others, 2023), which are sensitive to changing ocean temperatures (Shepherd and others, 2004). It has been argued in certain situations that only the total melt volume is important when calculating sea level contribution (e.g. Joughin and others, 2024), but this is certainly not a general rule. The distribution of melting under ice shelves can have a large impact on the dynamical changes upstream, and thus on the rates at which glaciers contribute to sea level (Walker and others, 2008). It has been shown that melt rate patterns can be as important as the magnitude in determining the modelled response of grounded ice (Gagliardini and others, 2010), and that certain locations around grounding lines and shear margins can be particularly sensitive to basal melt (Goldberg and others, 2019). Therefore, often-quoted mean melt rates over ice shelves do not sufficiently describe the forcing.

The most thorough way to represent basal melt patterns in future projections, and to ensure full interactivity between the ocean and ice sheet in predictive simulations, is by using coupled ice sheet and ocean models. However, the detail these can provide is limited by the resolution at which ocean models – usually running on a uniform rectangular grid – are able to simulate the system while remaining within reasonable limits of computational efficiency. Ice shelf basal melt rates near grounding lines require higher resolution than many ocean models can feasibly provide (McCormack and others, 2023), especially when considering anything larger than a regional-scale study, because melt rates derived from observations can vary at kilometre scales (Dutrieux and others, 2013). In many cases where interactive ice sheets have been coupled to the ocean at a circum-Antarctic or global scale, either the ocean model grid is not sufficiently fine to resolve small outlet glaciers and processes which affect the basal melting of ice shelves (e.g. Smith and others, 2021; Siahaan and others, 2022), or the ice sheet resolution is too coarse to track grounding line movement effectively (e.g. Ackermann and others, 2020; Pelletier and others, 2022).

To address this recognised capability gap in ice sheet-ocean modelling, the ice sheet model Úa (Gudmundsson and others, 2012) was paired with the ocean model FESOM (Wang and others, 2014) in a recently developed coupled framework (Richter and others, 2025). In Úa-FESOM both the ice sheet and ocean components run on finite-element unstructured meshes, allowing resolution in the ocean to be refined in areas of interest without having to compute solutions at the same fine resolution across the entire domain. This combination is the first of its kind among current coupled modelling frameworks, and overcomes the resolution limitations of existing setups to simulate a fully interactive global ice sheet-ocean system with sufficient spatial detail in regions of interest.

Here we follow on from the work of Richter and others (2025), in which the coupling process is described and verification carried out with forward simulations on both idealised and circum-Antarctic domains. Using the outputs from the first year of FESOM simulations alongside existing melt rate datasets derived from observations, we validate the melt rates produced by the ocean model for Antarctica. We run further ice sheet model simulations in order to show the importance of melt rate distribution and mesh resolutions, demonstrating why such a coupled setup is advantageous for modelling global systems.



# MODELS AND DATASETS

## Ocean model – FESOM

We use version 1.4 of the Finite Element Sea ice-Ocean Model (FESOM, Wang and others, 2014). This is a hydrostatic ocean model solving the primitive equations using a finite element method on a triangular mesh, and includes a sea ice component (Danilov and others, 2015). Thermodynamic interaction with the base of ice shelves is included via the three-equation melt parameterisation (Holland and Jenkins, 1999) as in Timmermann and others (2012). It has a history of use in stand-alone and coupled setups (e.g. Timmermann and Goeller, 2017; Naughten and others, 2018; Schourup-Kristensen and others, 2018), and participated in the Coupled Model Intercomparison Project 6 as a component of the Alfred Wegener Institute Climate Model (Semmler and others, 2020).

## Ice sheet model – Úa

We use version 2024b of Úa (Gudmundsson, 2024), a finite-element ice sheet model which solves the shallow shelf approximation (MacAyeal, 1989). The model solves the momentum and mass conservation equations in a coupled framework, i.e. by simultaneously solving for changes in velocity and ice thickness. It has been applied to numerous idealised and realistic use cases (e.g. De Rydt and others, 2021; Barnes and Gudmundsson, 2022; Morlighem and others, 2024), is well established in the cryospheric modelling community, and results based on the model have been submitted to various intercomparison projects (e.g.

Cornford and others, 2020; Seroussi and others, 2024).

## Melt rates derived from observations

To validate the basal melt rates from the Úa-FESOM coupled model, we have chosen three circum-Antarctic datasets to compare our outputs to.

Adusumilli and others (2020) estimated average basal melt rates for the period 2010-2018 based on satellite radar altimetry from the European Space Agency (ESA) mission CryoSat-2, ice velocities from Gardner and others (2018) and their novel model of variations in surface mass balance and firn density. Melt rates are provided on a regular grid with 500 m resolution.

Davison and others (2023) also use Cryosat-2 data, and estimate basal mass fluxes from 2010-2021 using ITS_LIVE (Gardner and others, 2019) for velocities and RACMO2.3p2 (Van Wessem and others, 2018) for firn density and surface mass balance. Melt rates are provided on a regular grid with 1 km resolution.

Paolo and others (2023) provide melt rates generated from the four ESA satellite radar altimetry missions ERS-1, ERS-2, Envisat, and CryoSat-2, using a novel data fusion approach and the Glacier Energy and Mass Balance model (GEMB, Gardner and others, 2023). We use the mean melt rates provided at a resolution of 1920 m.

These observationally-derived melt rates differ from each other due to varying input data and methodology. They are not a perfect picture of true melt rates, as assumptions have necessarily had to be used in their calculations of melt rate from observed surface properties. There are also gaps in their coverage, for which interpolation and extrapolation must be used in order to provide complete melt rates over ice shelves. Despite this, they are very useful products based on real data and are the best available estimates for the large-scale distribution of melt rates around Antarctica. Throughout the text, we refer to these three datasets by the first author names Adusumilli, Davison and Paolo.

# EXPERIMENTS

## Model setup

We use the exact coupling procedure and ocean model setup described in Richter and others (2025). The horizontal mesh resolution in FESOM ranges from 340 km in the middle of the oceans far away from Antarctica to 2 km underneath ice shelves. There are 100 levels in the vertical, with a resolution of 10-30 m under ice shelves. The geometry for FESOM was taken from RTopo-2 global bathymetry data (Schaffer and others, 2016), with ice shelves based on BedMachine Antarctica (Morlighem and others, 2020). The simulations were started from the Antarctic spin-up state described in Richter and others (2025), in which the ocean begun at rest with hydrography from the World Ocean Atlas (WOA18) extrapolated into ice shelf cavities, and was forced by daily ERA-Interim atmospheric reanalysis (Dee and others, 2011) for 1979-2018. This initial adjustment phase was included to mitigate issues caused by instabilities reported in previous coupled modelling work. The same reanalysis cycle was then used to force the forward simulation, of which we use only the outputs after the first year. Simulations were performed using two different values for the drag coefficient at the ice shelf base ($C_d$), of $1.25 \times 10^{-2}$ and $2.5 \times 10^{-2}$. This coefficient is used in calculating momentum and turbulent exchange through the ice-ocean boundary layer, and thus impacts the magnitude of melt rates calculated. Such parameters are commonly used to tune melt rates within coupled model setups, but its effect on melt rate distribution is largely untested, which is why we include it as a variable quantity here.

The coupler transfers the outputs from FESOM and converts the thermal forcing into a basal melt rate for the ice shelves, which is then interpolated onto Úa's mesh. Here is where our experiments diverge from those of Richter and others (2025). We have generated new Antarctic meshes for Úa, with a resolution of 20 km at the centre of the continent and refining down to 1.5 km around the grounding lines and areas of high observed ice velocities. We use two meshes which differ in their resolution on the ice shelves themselves. Ice Mesh 1 is generated using the same conditions everywhere, resulting in the largest elements in the middle of the Ross Ice Shelf – far from the grounding line – having element edges around 15 km in length. Ice Mesh 2 is generated with exactly the same conditions for grounded ice, but a smaller target element size on the ice shelves, where the edge lengths of the largest elements are now only 3-4 km. A comparison of these meshes on selected ice shelves of varying sizes is shown in Fig. 1. For our purposes simulations

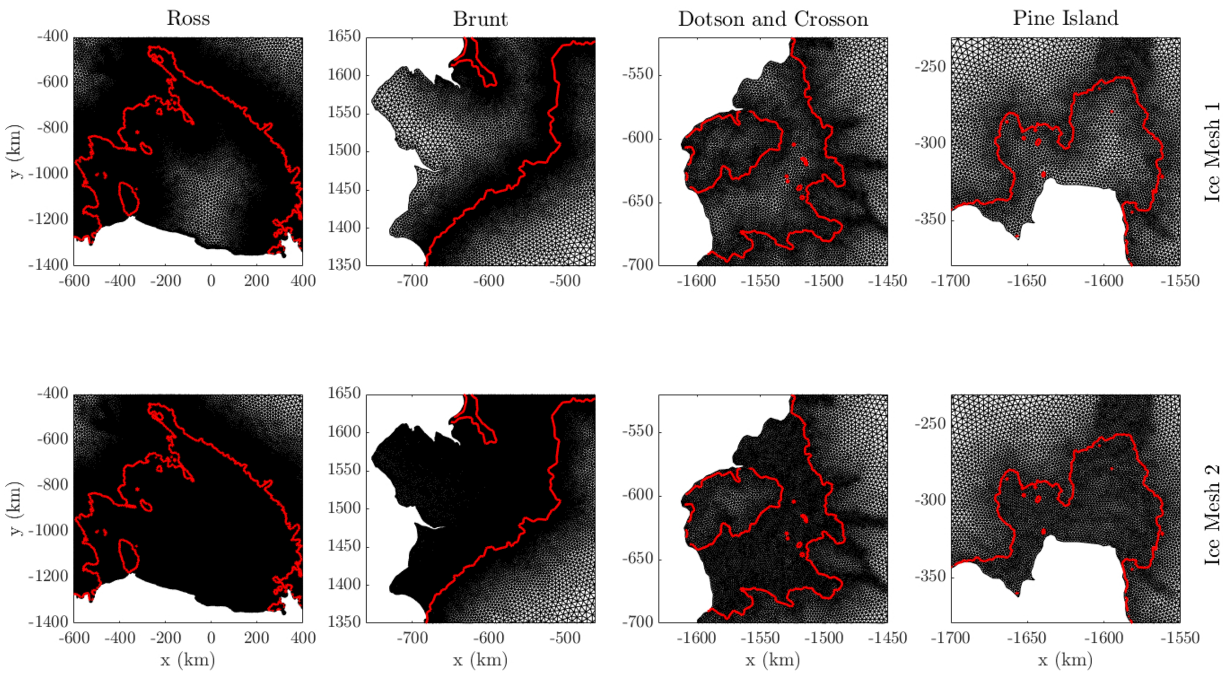


**Fig. 1.** A comparison of the two ice sheet model meshes used in Úa, zoomed into selected ice shelves of varying scales. Ice Mesh 1 on the top row uses the same criteria everywhere, while Ice Mesh 2 on the bottom row uses smaller target element sizes on ice shelves.



were run on a single computational core, but these meshes are very large and it would be impractical to run long-term simulations (decade to century scale) on them without some parallelisation of the ice sheet model. A model inversion was carried out in order to infer values for the flow rate factor $A$ of Glen's law and basal sliding parameter $C$ of Weertman's law, which are used in the forward simulations. Details on this process in Úa can be found in previously published work (e.g. Barnes and others, 2021).

## Simulations

We run simulations in Úa for one year. For the purposes of this work, we then stop the coupling procedure before any data is transferred back to FESOM. The focus of this work is melt rates provided by the ocean model and other sources for the present day, rather than the effects on and of future evolution of the geometry. In addition to those using our two FESOM outputs, further simulations are run in Úa forced by the three observationally-derived melt rates, and also by depth-dependent melt rates defined by

$$M = \begin{cases} 0 & \text{if } z \geqslant 0 \\ -\frac{M_{\max}}{500} z & \text{if } 0 > z > -500 \\ M_{\max} & \text{if } z \leqslant -500, \end{cases} \tag{1}$$

where $M_{\max}$ is a maximum melt rate for which we use value of $50\,\mathrm{m\,a^{-1}}$. We also use $M_{\max} = 0\,\mathrm{m\,a^{-1}}$ as a control to account for model drift, and in parts of our analysis consider outputs from all other simulations in terms of how they differ from the control.

To fairly assess the impact of melt distribution, we run sets of simulations on Ice Mesh 1 in which the melt forcings are normalised to produce the same total melt volume across four ice shelf regions; Vigrid/Nivl, Amery, Ross and Dotson/Crosson. In this way, we directly address the importance of melt rate distributions on these ice shelves without the influence of a differing overall melt magnitude . We choose to match the total melt volume of the Adusumilli data, which produces close to the median total melt among our melt rate products on three of our four chosen regions.

In order to assess potential impacts of ocean model resolution, we also regrid the FESOM outputs by interpolating them onto two regular grids of 20 km and 5 km, hereafter referred to as Grid20 and Grid5. These roughly correspond to common ocean model resolutions of 1-degree and $\frac{1}{4}$-degree around Antarctica, respectively. The gridded melt rates are then used in the same way as the original model output – interpolated onto the ice model mesh to force the simulation.

## Analysis methods

As ice shelves around Antarctica are not all the same, we evaluate the similarity of spatial patterns on 50 individual ice shelves, with Ross Ice Shelf split into East and West sections. The ice shelf boundaries are from the MEaSUREs dataset (Mouginot and others, 2017), and a labelled map showing the locations of the ice shelves we look at is displayed in Fig. 2.

To investigate the similarity between our modelled melt rates and those derived from observations, we

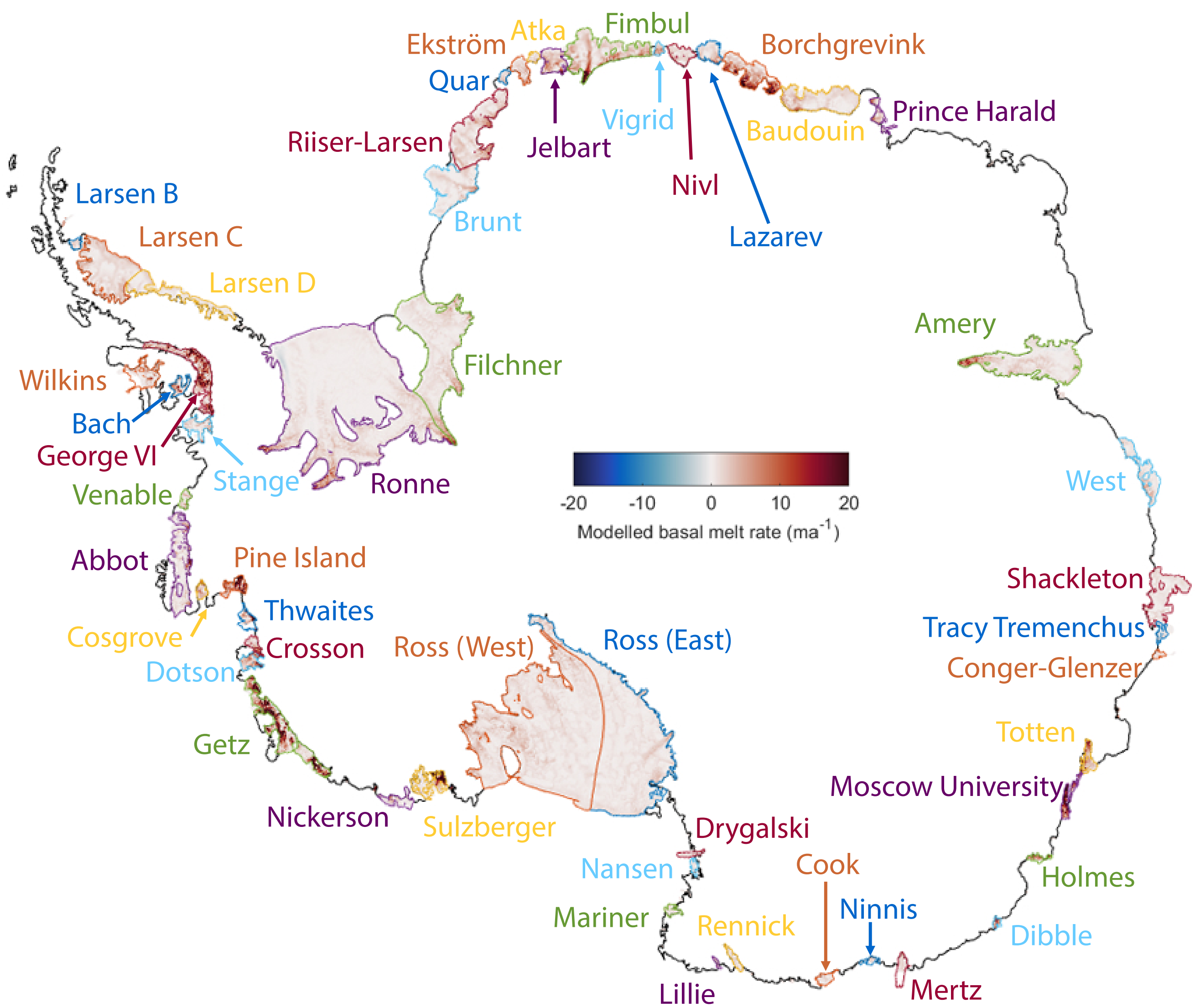


**Fig. 2.** A map of Antarctica labelled with the 50 ice shelves included in our analysis. Basal melt rates of ice shelves are from FESOM with $C_d = 1.25 \times 10^{-2}$.

choose to calculate Pearson's Correlation Coefficient $r$ (PCC, Pearson, 1895), a commonly used measure of linear association between two variables (Swinscow and others, 2002), given by

$$r = \frac{\Sigma(x_i - \bar{x})(y_i - \bar{y})}{\sqrt{\Sigma(x_i - \bar{x})^2 \Sigma(y_i - \bar{y})^2}}, \tag{2}$$

where $x_i$ and $y_i$ are the individual values of two variables, $\bar{x}$ and $\bar{y}$ are the mean values of each variable. We interpolate all melt rate datasets and FESOM outputs onto the ice model meshes for comparison. Since our values are taken from an unstructured mesh, we use a modified correlation which weights the calculation based on the mesh element areas. Classifying correlation values is not a precise exercise, and labels given to indicate the strength of correlation vary between studies. We use the labels of Swinscow and others (2002), which suggests $|r| \geqslant 0.6$ as a "strong" correlation and $0.4 \leqslant |r| < 0.6$ as "moderate". The PCC is not a perfect measure and can be greatly affected by outliers, especially if the sample size is small (Armstrong, 2019). For this reason we do not rely on it entirely, and we also visually inspect the outputs.

# RESULTS

## Correlation with observationally-derived basal melt

Table 4 shows the correlation between each of the model melt rates (from FESOM and the depth-dependent parameterisation) and the three observationally-derived melt rates on Ice Mesh 1, for our chosen ice shelves. The colours display the strength of correlations, with red being positive and blue negative, and paler shades indicating lower correlation. The number of elements used to calculate the correlation in each case are also displayed, to demonstrate that these are not small sample sizes.

The melt rates under ice shelves show a range of responses to varying $C_d$. On several ice shelves – such as Filchner, Ronne, Fimbul, Amery, Sulzberger, Crosson, Pine Island and Stange – FESOM shows fairly high positive correlation with all three observationally-derived datasets using both $C_d$ values. Conversely, on the small ice shelves Vigrid and Nivl on the Dronning Maud Land coast a negative correlation is seen when using $C_d = 1.25 \times 10^{-2}$, but becomes positive when using $C_d = 2.5 \times 10^{-2}$. This demonstrates that in addition to the effects on the magnitude of melt, there is in some locations a sensitivity of melt rate distribution to the parameter used to tune the ocean model outputs. Table 5 shows correlation coefficients between the two FESOM outputs, and also between each pair of observationally-derived datasets. On many ice shelves, there is a high level of agreement between the different datasets, but this is not the case everywhere. Further examples can be seen here of ice shelves where different values of $C_d$ in FESOM lead to uncorrelated distributions of melt, and in one case a moderate negative correlation on Atka.

Overall, 12 of the ice shelves have a strong positive correlation between at least one pair of modelled and observationally-derived melt rates, and a further 16 have a moderate correlation. This means that overall more than half of the ice shelves in our analysis (55%) have a modelled melt rate from FESOM with at least moderate positive correlation to an observationally-derived melt rate, indicating a significant level of agreement. The FESOM melt rates do not always correlate well with those from the observationally-derived datasets, however. For example, almost no correlation is seen between FESOM and any of the observationally-derived datasets on Larsen D, Borchgrevink, Rennick, Lillie, Drygalski or Wilkins. In a few cases negative correlation is seen – notably on Nansen with the Paolo datset where this is classed as moderate for both choices of $C_d$ – indicating that the model output is directly contradictory to the data in these cases. Where the three observationally-derived datasets disagree, our modelled melt rates from FESOM do not favour any particular one. On Larsen B, for example, the FESOM melt rates correlate with those of Paolo but not with the other datasets. Meanwhile, on Dotson the strongest correlation is with the Davison melt rates and on Mertz we find a high correlation with both Adusumilli and Davison, but not with Paolo.

The FESOM outputs display much higher agreement to observationally-derived datasets than the depth-dependent melt rate. Looking at the outputs of the simple paramaterisation, we find only ten ice shelves – 20% of the total – to have at least moderate positive correlation with any of the observational datasets, and only one instance of a strong positive correlation with the Paolo melt rates on Crosson.

Table 6 shows the same information as Table 4, but for Ice Mesh 2, which has a higher resolution on the ice shelves. There are no major differences between the correlation results on the two meshes, although only 49% of the ice shelves have at least moderate positive correlation between a FESOM output and an observational dataset using this mesh, which is slightly lower than on Ice Mesh 1. This could indicate that some processes affecting melt rate distributions at length scales below the element sizes on Ice Mesh 1 are not being represented in the model.

Table 7 shows correlation coefficients between the observationally-derived datasets and the regridded FESOM melt rates, on Ice Mesh 2. Patterns in these results vary between ice shelves; for example there is stronger correlation with observationally-derived melt rates on Stange using Grid5, but stronger correlation on Thwaites using Grid20. In general we see slightly stronger correlation using Grid5 than Grid20 with Adusumilli and Davison, but weaker correlation with Paolo. This may be connected to the fact that the Paolo data is provided on a coarser grid than the other datasets, although it is still at a higher resolution than Grid5.

## Visual inspection of melt rate distributions

In several instances the modelled melt rates from FESOM have a higher magnitude than any observed values. This is seen for George VI and Bach in the Antarctic Peninsula, along with Abbot, Venable and Cosgrove. It is also the case along sections of the coast around Dronning Maud Land and on Getz, Nickerson and Sulzberger. However, we know that magnitudes can be tuned by use of ocean model parameters such as $C_d$, and in this work we are focused on the spatial distributions of the melt.

We present in detail the melt rate distributions from all observationally-derived datasets and modelled/parameterised melt on four regions, chosen to represent areas with different correlation behaviour as well as a variety of ice shelf sizes and locations around the Antarctic coastline. Vigrid and Nivl ice shelves (Fig. 3) on the Dronning Maud Land coast stand out in the correlation tables due to the FESOM outputs having completely opposite correlations – positive or negative – depending on the choice of $C_d$. Amery (Fig. 4), in East Antarctica, is a large confined ice shelf which displays high correlation between FESOM and observationally-derived datasets in all cases, but no correlation with a depth-dependent melt rate. Ross Ice Shelf (Fig. 5) is the largest in the world by surface area. Correlation values here are low in most cases. Crosson Ice Shelf (Fig. 6) uniquely has moderate or strong positive correlation between every pair of modelled and observed melt rates, including the depth-dependent parameterisation. Its neighbour Dotson also displays universally positive correlation, although not as strong. This small sample of ice shelves serve as examples to demonstrate several wider observations without the impracticality of plotting every single ice shelf around Antarctica. Our melt rate fields for the entirety of Antarctica are available to be examined

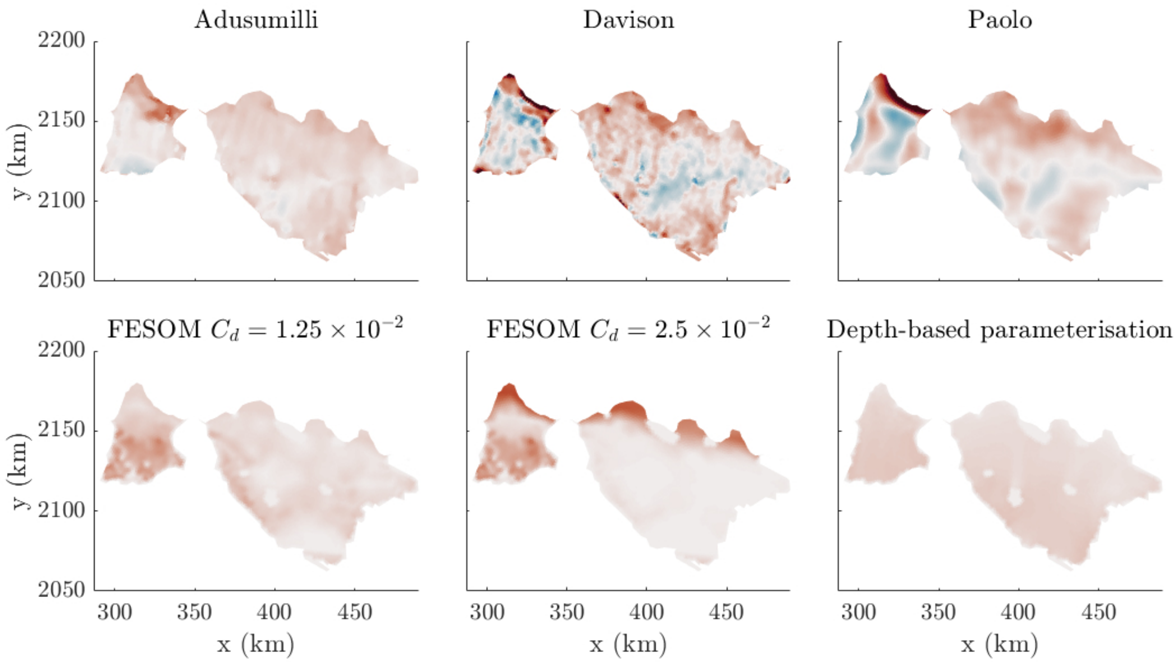


**Fig. 3.** Melt rate distributions on Vigrid and Nivl ice shelves, for the three observationally-derived datasets, the two FESOM outputs and the depth-dependent melt parameterisation. Red represents melting and blue refreezing, with darker shades of either colour being higher in magnitude. Colourbars are not included in the figure, as the values have been normalised to represent the same total melt across the ice shelf, and are therefore not intended for comparison of the magnitude of the outputs.



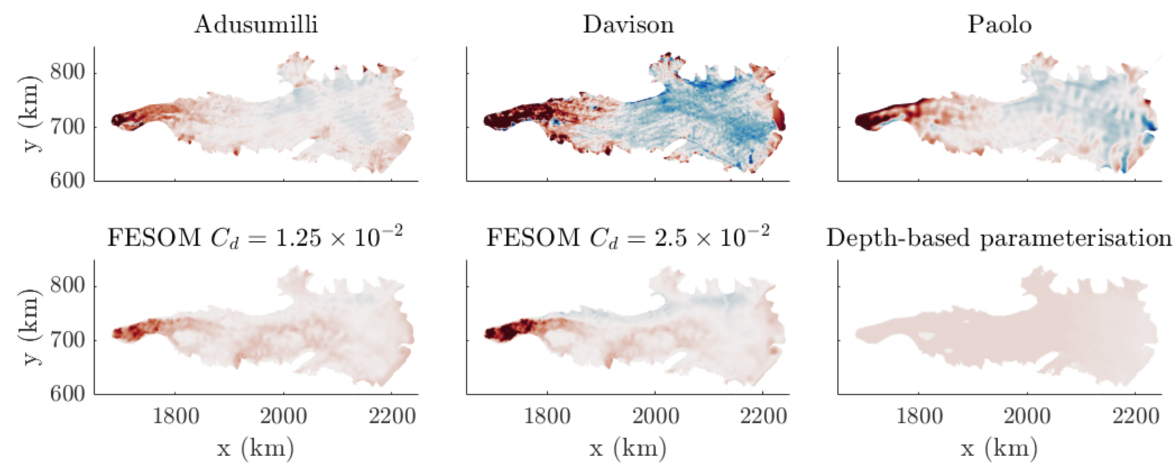


**Fig. 4.** As in Fig. 3, for Amery Ice Shelf.

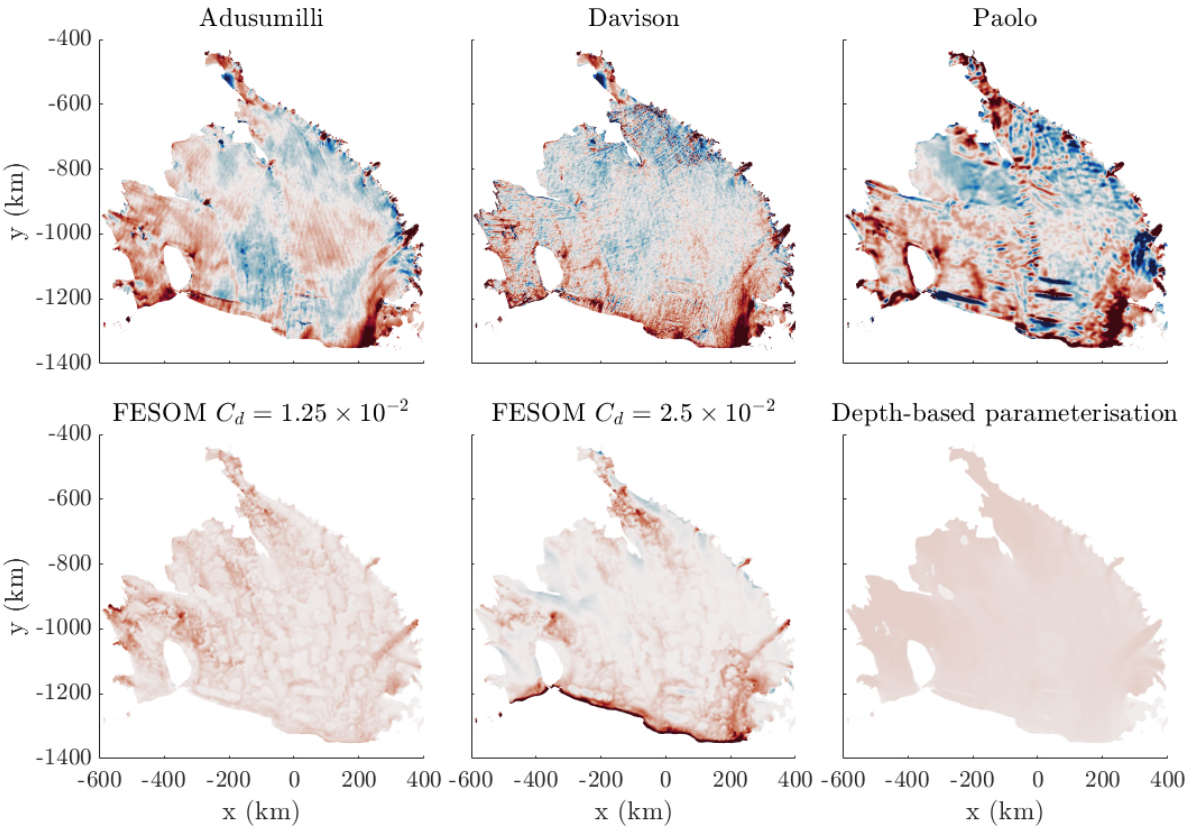


**Fig. 5.** As in Fig. 3, for Ross Ice Shelf.

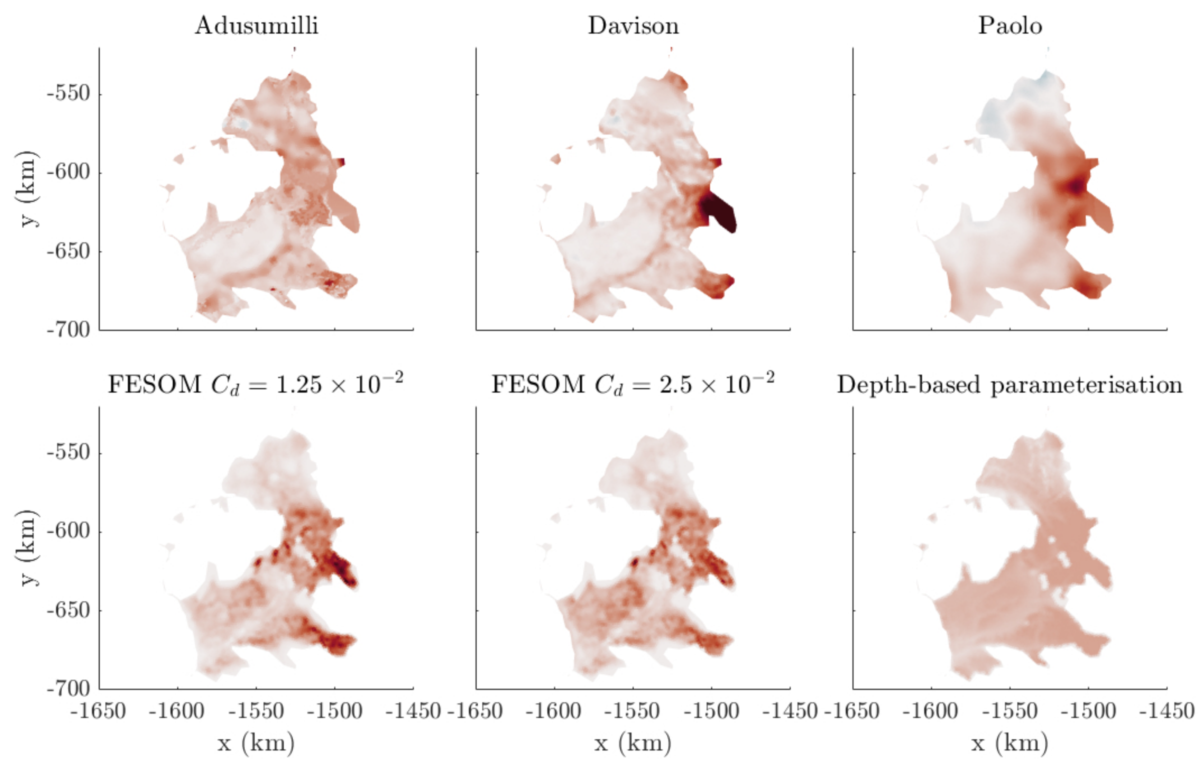


**Fig. 6.** As in Fig. 3, for Dotson and Crosson ice shelves.

at the reader's leisure (Barnes, 2026).

Important features of patterns in the melt rates are similar across several large ice shelves. For example, all modelled and observed melt rates have high melting in the narrow region of Amery (Fig. 4) near the grounding line, and refreezing occurring down the Eastern side. The refreezing is better reproduced by FESOM using the higher value of $C_d$, although still not as pronounced as in the observationally-derived datasets. Similarly, areas of refreezing on Ross (Fig. 5) and Filchner-Ronne are better represented when using the higher $C_d$, but not to the full extent seen in observations. The depth-dependent parameterisation does not produce any refreezing, having a minimum melt rate of $0\,\mathrm{m\,a^{-1}}$.

High melt rates are often seen in narrow outlets with deep ice-shelf draft, where glaciers and ice streams feed larger ice shelves. In addition to the examples in our figures of Amery (Fig. 4), Ross (Fig. 5), Dotson and Crosson (Fig. 6), this can also be seen in all modelled and observed datasets for glaciers flowing into Filchner-Ronne as well as Brunt, Jelbart and Fimbul along the Dronning Maud Land coast. The depth-dependent melt rate does not include this fine detail, simply displaying a gradual gradient from higher melt near the grounding line to lower melt near the ice front without much variability.

Use of the higher value of $C_d$ in FESOM often results in a narrow band of higher melting at the ice front, as can be seen on Ross (Fig. 5), Vigrid and Nivl (Fig. 3). Conversely, on Amery (Fig. 4) a band of higher melt is more evident at the ice front when using the lower value of $C_d$. This is a major difference on the ice shelves where the two FESOM outputs do not display strong or moderate positive correlation. In some cases, notably on Ross and Filchner-Ronne, such a band of high melt rates can be seen in the observationally-derived melt rates. In other cases there is no match with the observations, or at least not with all datasets. The Davison melt rates include bands of higher melt rates at the fronts of several glaciers which the other datasets do not, as can be seen on Amery. A reason for this difference between the observationally-derived and modelled outputs could be that warm surface water penetrates into the cavities under ice shelves in the summer months. We are looking at model results from the end of the year, in December, and so this summer signal would be seen. It may however show up to different extents on different ice shelves in the annual mean observations.

| Variable for which | $C_d = 1.25 \times 10^{-2}$ | | | $C_d = 2.5 \times 10^{-2}$ | | |
|---|---|---|---|---|---|---|
| difference calculated | FESOM mesh | Grid5 | Grid20 | FESOM mesh | Grid5 | Grid20 |
| VAF change | 4.5 % | 3.8 % | 0.4 % | 3.5 % | 1.8 % | 1.4 % |
| Grounded area change | 10.4 % | 11.3 % | 8.3 % | 7.4 % | 7.5 % | 1.9 % |

**Table 1.** Percentage difference of VAF and grounded area changes after one year of simulation when using Ice Mesh 2 compared to Ice Mesh 1, for the full range of melt rate data gridding options.

## Effects of resolution in a forward simulation

After our year of forward simulation, we look at additional changes in volume above flotation (VAF) and grounded area across the entire domain using different mesh and data resolutions, compared to the control simulation. In general, using a higher mesh resolution either for the ice model or for the input melt rate data leads to faster changes in the ice sheet.

With the same input melt rates from FESOM, simulations in Úa run on Ice Mesh 2 experience up to 4.5% more VAF loss and up to 11.3% more change in grounded area across the domain over the initial year than the simulations on Ice Mesh 1. This difference is greatest when the input melt rates are either the original FESOM outputs or the Grid5 data. The results of this comparison when using the Grid20 melt rates are generally more similar. It is also notable that larger differences are generally seen when FESOM uses $C_d = 1.25 \times 10^{-2}$. Grounded area changes are consistently more sensitive to the ice model resolution than VAF changes in the first year, but changes to the grounding line could lead to additional melting and more ice loss as the ice sheet evolves further. These results are summarised in Table 1.

Regridding the FESOM melt rates is a proxy for ocean model resolution. Grid20 represents a 1-degree ocean grid, while Grid5 represents a $\frac{1}{4}$-degree grid. Compared to using FESOM's original output, using Grid20 results in up to 8.5% less VAF loss and up to 8.3% less grounded area change. Results are generally more similar when using Grid5, which is closer in resolution to the original FESOM mesh, and when using Ice Mesh 1, which is coarser over the ice shelves. These results are summarised in Table 2.

The importance of mesh resolution in ocean and ice sheet models is well known, with a recent example showing instances of grounding line migration in Úa only captured with resolutions less than 2 km (Sun

| Variable for which difference calculated | $C_d = 1.25 \times 10^{-2}$ | | | | $C_d = 2.5 \times 10^{-2}$ | | | |
|---|---|---|---|---|---|---|---|---|
| | Ice Mesh 1 | | Ice Mesh 2 | | Ice Mesh 1 | | Ice Mesh 2 | |
| | Grid5 | Grid20 | Grid5 | Grid20 | Grid5 | Grid20 | Grid5 | Grid20 |
| VAF change | 0.6 % | -4.8 % | -0.1 % | -8.5 % | 3.5 % | -1 % | 1.9 % | -5.6 % |
| Grounded area change | 0.2 % | -6.4 % | 1 % | -8.2 % | 2 % | -3.4 % | 2.1 % | -8.3 % |

**Table 2.** Percentage difference of VAF and grounded area changes after one year of simulation when using regridded FESOM outputs compared to outputs on the original mesh, for both ice sheet model meshes.

and Gudmundsson, 2026). Of course, in all modelling work a balance must be found between resolution and computational efficiency. This is where Úa-FESOM is a very promising setup for future predictive studies. The triangular mesh structure shared by both components of the coupled model allows for much finer detail to be modelled than when using regular grids for a similar computational cost, whether on regional or continental-scale domains.



## Effects of melt distribution in a forward simulation

After one year of simulation, we inspect the results of a set of experiments using melt rate distributions normalised such that they provide the same total melt volume over certain ice shelves. For each of our four chosen regions detailed previously, we choose the Adusumilli data as our reference and multiply each of the other forcing products by a factor which causes the same total melt volume. The distributions are those displayed in Figs. 3-6, and the total annual melt volumes are 10.42 $km^3$ for Vigrid and Nivl, 53.84 $km^3$ for Amery, 64.15 $km^3$ for Ross, and 54.47 $km^3$ for Dotson and Crosson. In all, 24 simulations were run for the analysis in this section; one for each of the six melt distributions on each of the four ice shelf regions. These simulations used Ice Mesh 1 and the FESOM outputs on their original mesh. We calculate the additional changes to VAF and grounded area in the relevant catchment basins of the ice shelves in question (as defined by Mouginot and others (2017)), compared to the control simulation; that is, the changes which can be fully attributed to choice of ice shelf basal melt distribution. A summary of results is shown in Table 3.

As we are only looking at the differences in VAF and grounded area over one year in the catchments of specific ice shelves, the magnitudes we see in our results are small. However, in proportional terms, there are very large differences between the impacts of different melt rate products which would likely propagate

| Melt rate distribution | Additional VAF change (km$^3$) | | | | Additional GA change (km$^2$) | | | |
|---|---|---|---|---|---|---|---|---|
| | V&N | Amery | Ross | D&C | V&N | Amery | Ross | D&C |
| Adusumilli | -0.03 | -0.53 | -0.78 | -0.32 | -3.97 | -5.08 | -27.01 | -2.82 |
| Davison | -0.09 | -1.38 | 0.75 | -0.60 | -7.25 | -22.74 | 19.64 | -6.05 |
| Paolo | -0.03 | -0.69 | 0.26 | -0.42 | -0.96 | -9.35 | -23.67 | -3.78 |
| FESOM ($C_d = 1.25 \times 10^{-2}$) | -0.06 | -0.43 | 1.29 | -0.43 | -3.80 | -2.85 | -28.40 | -5.48 |
| FESOM ($C_d = 2.5 \times 10^{-2}$) | -0.05 | -0.30 | 0.97 | -0.32 | -2.03 | -0.13 | -4.21 | -3.22 |
| Depth-based parameterisation | -0.07 | -0.32 | 1.42 | -0.54 | -5.94 | -8.10 | -24.18 | -4.29 |

**Table 3.** The additional VAF and grounded area (GA) changes compared to a control run, in the catchment area of the selected ice shelf region when using weighted melt rates to produce the same total melt volume on the ice shelf. V&N is Vigrid and Nivl, D&C is Dotson and Crosson.



into greater magnitudes over a longer simulation. The most extreme example is the Davison melt distribution on Amery causing 175 times more loss of grounded area than FESOM outputs with $C_d = 2.5 \times 10^{-2}$ ($22.74\,\mathrm{km}^2$ compared to $0.13\,\mathrm{km}^2$), and almost 5 times the amount of VAF loss. The Davison dataset is particularly notable as an outlier on Amery, where it produces a large amount of refreezing and thus the magnitudes of melting areas are amplified during the normalisation to equalise the total melt volume with the other datasets. Therefore, there is higher melt in the narrow section at back of the ice shelf than in the other datasets. While admittedly an extreme case, this is a valuable demonstration of the importance of considering melt rate distribution rather than relying entirely on total melt volume across an ice shelf. On Ross ice shelf, there are instances of different melt rate distributions causing changes of opposite signs, showing that differing distribution of the same total melt volume has the potential to affect whether the ice sheet gains or loses mass. Since these results used Ice Mesh 1, the differences could potentially be larger if the mesh were refined over the ice shelves as in Ice Mesh 2.

In Fig. 7 we plot the differences in ice speed and thickness between the simulations which displayed the most different VAF and grounded area changes. On the slow-flowing Vigrid and Nivl ice shelves, the differences in thickness due to melt distributions do not significantly impact the ice speed. For the other three regions, where the ice flows faster, the largest differences are seen on the floating ice where the differences in melt rate distributions have the most immediate impact. Differences in ice speed on all the ice shelves vary on the order of $10\,\mathrm{m\,a}^{-1}$, and up to around $50\,\mathrm{m\,a}^{-1}$ on some parts of Crosson. Similar

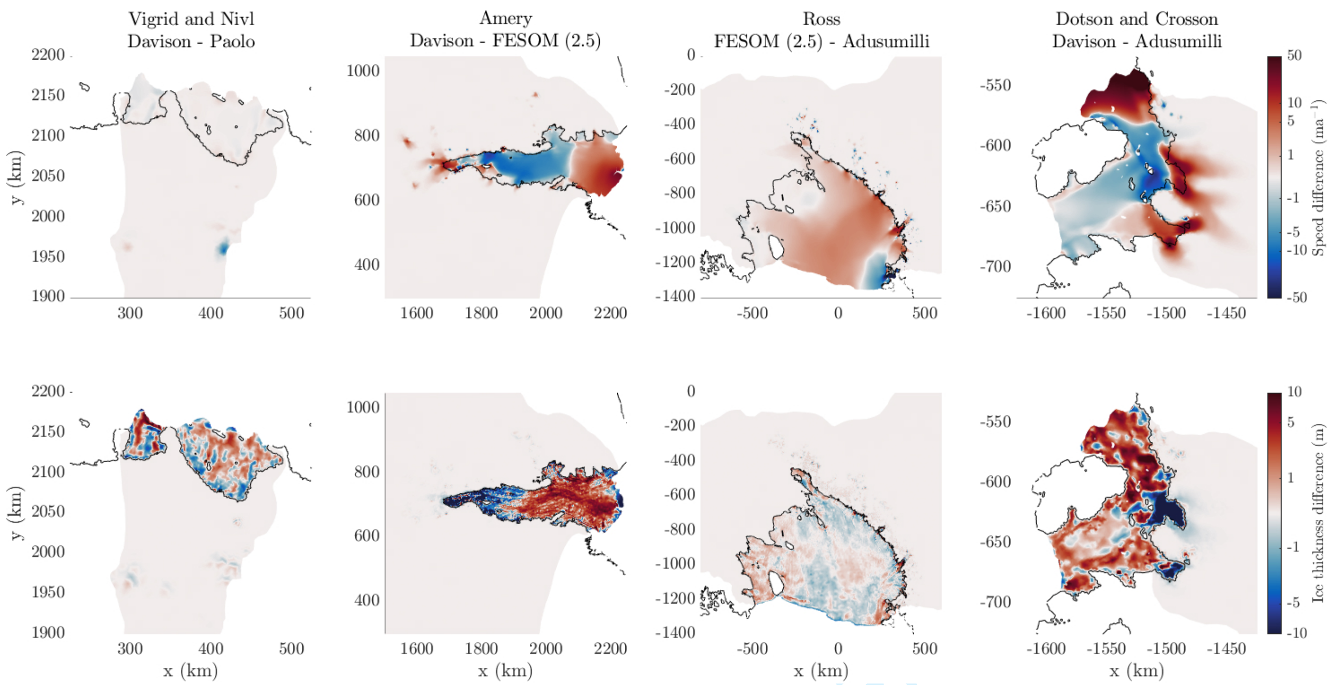


**Fig. 7.** Differences in ice speed and thickness after one year, between pairs of simulations forced by different melt distributions, selected due to having the greatest differences in VAF and grounded area changes on the selected ice shelf region. The melt rate distributions are normalised to produce the same total melt volume, and are pictured in Figs. 3-6. FESOM (2.5) refers to the FESOM melt rates using $C_d = 2.5 \times 10^{-2}$.

speed differences are seen over grounded ice in the glaciers flowing out onto Amery, Dotson and Crosson, where the Davison melt distribution produces higher melt rates at the grounding lines and drives faster flow. Proportionally, speed differences between simulations using different melt distributions are on the order of 2-3% of the initial ice speed across much of Amery and Crosson, with peaks reaching around 10% in a few locations at the grounding lines.

## CONCLUSIONS

The results of our correlation analysis validate the spatial distributions of melt rates produced by FESOM – the ocean component of our coupled model – against data derived from observations, when interpolated onto the mesh used by Úa – the ice component. We have shown that melt rate patterns produced for a majority of Antarctic ice shelves are at least moderately correlated (Pearson's Correlation Coefficient $r \geqslant 0.4$) with at least one observationally-derived melt rate and using at least one of the two values we tested for the turbulent exchange coefficient. Correlation is far better when using FESOM outputs rather than a depth-dependent melt rate, demonstrating the value of a coupled modelling approach compared to simple parameterisations.



An obvious issue with the FESOM outputs is that, while they perform better than a simple parameterisation, the quality of any one output is not universal. This would be true of melt rates derived from any ocean model. The value of $C_d$ can be used to "tune" the model to match magnitudes of observed melt in a specific region. However, this parameter would need to be set to different values to best represent different ice shelves. We show here that changing this value not only alters the magnitude of the melt rate, but can also cause significant changes in how the melt is distributed across an ice shelf in some cases. This highlights a localised sensitivity to varying ocean model parameters. Those ice shelves in our analysis for which melt rate distributions do not correlate with observations may do so after tuning $C_d$ to capture local behaviour. As a result, we suggest that future simulations of the whole of Antarctica should consider varying the drag coefficient – or any other tuning parameter – spatially rather than implementing it as a constant, in order to capture the important differences between individual ice shelves as in, for example, Nakayama and others (2017). While set up initially for full circum-Antarctic simulations, other use cases for Úa-FESOM may be in regional studies, where local magnitudes and distributions of present-day melting can be more closely reproduced by tuning the ocean model parameters.

Unsurprisingly, model resolution is shown to be an important consideration for both the ocean and ice sheet components. Higher resolution in either the ice sheet model or the melt rate forcing from the ocean model leads to larger changes in VAF and grounded area over the first year of model simulation, with differences on the order of 10% compared to our lower resolution meshes. This will likely propagate into future years of simulation in longer runs.

By running simulations with different melt rate products normalised to produce the same total magnitude of melt over ice shelves, we show that the distribution of melt can make a large difference to the evolution of the ice sheet. We show that differences in speed on the order of $10\,\mathrm{m\,a^{-1}}$ are seen on the larger ice shelves, with these speed differences propagating inland. The largest differences, around 10% of the ice speed, are at the grounding lines of specific glaciers where particularly high melt is produced by some distributions. This emphasises the greater influence of melt in specific areas, and thus the importance of ice shelf basal melt rate distributions in driving the evolution of ice sheets.

To summarise, in this work we have demonstrated that the Úa-FESOM coupled ice sheet-ocean model does a good job of reproducing observed melt rate distributions, achieving at least moderate correlation on half of the ice shelves in our study. We have shown that melt rate distributions can be greatly affected by the choice of the drag coefficient $C_d$, which is used to tune the modelled melt rates, and thus localised tuning could produce good results for those ice shelves on which we did not match observations. We have also demonstrated how much melt distributions matter, and the importance of model resolution in the ice sheet-ocean modelling context. To address both of these factors in future predictive studies, we encourage further work with Úa-FESOM and recommend development and use of other such coupled model setups with triangular mesh structures in both components.

## ACKNOWLEDGEMENTS

This work was funded by the EU Horizon 2020 project PROTECT (grant no. 869304), with further support from Novo Nordisk Foundation grant NNF23OC0081251. Thanks to Ole Richter for providing valuable training and assistance with setting up and running FESOM, and to the Nationales Hochleistungsrechnen (NHR) alliance for providing computer resources through project hbk00097.

# REFERENCES

Ackermann L, Danek C, Gierz P and Lohmann G (2020) AMOC recovery in a multicentennial scenario using a coupled atmosphere-ocean-ice sheet model. *Geophys. Res. Lett.*, **47**(16), e2019GL086810

Adusumilli S, Fricker HA, Medley B, Padman L and Siegfried MR (2020) Interannual variations in meltwater input to the Southern Ocean from Antarctic ice shelves. *Nature Geoscience*, **13**(9), 616–620

Armstrong RA (2019) Should Pearson's correlation coefficient be avoided? *Ophthalmic and Physiological Optics*, **39**(5), 316–327

Barnes JM (2026) Model data and output to accompany "The importance of ice shelf melt rate distributions in modelling of Antarctic ice loss" by Barnes et al. `https://doi.org/10.5281/zenodo.22233394`

Barnes JM and Gudmundsson GH (2022) The predictive power of ice sheet models and the regional sensitivity of ice loss to basal sliding parameterisations: a case study of Pine Island and Thwaites glaciers, West Antarctica. *The Cryosphere*, **16**(10), 4291–4304

Barnes JM, Dias dos Santos T, Goldberg D, Gudmundsson GH, Morlighem M and De Rydt J (2021) The transferability of adjoint inversion products between different ice flow models. *The Cryosphere*, **15**(4), 1975–2000

Cornford SL, Seroussi H, Asay-Davis XS, Gudmundsson GH, Arthern R, Borstad C, Christmann J, Dias dos Santos T, Feldmann J, Goldberg D, Hoffman MJ, Humbert A, Kleiner T, Leguy G, Lipscomb WH, Merino N, Durand G, Morlighem M, Pollard D, Rückamp M, Williams CR and Yu H (2020) Results of the third Marine Ice Sheet Model Intercomparison Project (MISMIP+). *The Cryosphere*, **14**(7), 2283–2301 (doi: 10.5194/tc-14-2283-2020)

Danilov S, Wang Q, Timmermann R, Iakovlev N, Sidorenko D, Kimmritz M, Jung T and Schröter J (2015) Finite-element sea ice model (FESIM), version 2. *Geoscientific Model Development*, **8**(6), 1747–1761

Davison BJ, Hogg AE, Gourmelen N, Jakob L, Wuite J, Nagler T, Greene CA, Andreasen J and Engdahl ME (2023) Annual mass budget of Antarctic ice shelves from 1997 to 2021. *Science Advances*, **9**(41), eadi0186

De Rydt J, Reese R, Paolo FS and Gudmundsson GH (2021) Drivers of Pine Island Glacier speed-up between 1996 and 2016. *The Cryosphere*, **15**(1), 113–132

Dee DP, Uppala SM, Simmons AJ, Berrisford P, Poli P, Kobayashi S, Andrae U, Balmaseda M, Balsamo G, Bauer dP and others (2011) The ERA-Interim reanalysis: Configuration and performance of the data assimilation system. *Quarterly Journal of the royal meteorological society*, **137**(656), 553–597

Dutrieux P, Vaughan DG, Corr HF, Jenkins A, Holland PR, Joughin I and Fleming A (2013) Pine Island glacier ice shelf melt distributed at kilometre scales. *The Cryosphere*, **7**(5), 1543–1555

Gagliardini O, Durand G, Zwinger T, Hindmarsh R and Le Meur E (2010) Coupling of ice-shelf melting and buttressing is a key process in ice-sheets dynamics. *Geophysical Research Letters*, **37**(14)

Gardner AS, Moholdt G, Scambos T, Fahnstock M, Ligtenberg S, Van Den Broeke M and Nilsson J (2018) Increased West Antarctic and unchanged East Antarctic ice discharge over the last 7 years. *The Cryosphere*, **12**(2), 521–547

Gardner AS, Fahnestock MA and Scambos TA (2019) MEaSURes ITS_LIVE Regional Glacier and Ice Sheet Surface Velocities, Version 1 (doi: 10.5067/6II6VW8LLWJ7)

Gardner AS, Schlegel NJ and Larour E (2023) Glacier Energy and Mass Balance (GEMB): a model of firn processes for cryosphere research. *Geoscientific Model Development*, **16**(8), 2277–2302

Goldberg D, Gourmelen N, Kimura S, Millan R and Snow K (2019) How accurately should we model ice shelf melt rates? *Geophysical Research Letters*, **46**(1), 189–199

Gudmundsson G, Krug J, Durand G, Favier L and Gagliardini O (2012) The stability of grounding lines on retrograde slopes. *The Cryosphere*, **6**(6), 1497–1505

Gudmundsson GH (2024) GHilmarG/UaSource: Ua2024b (Version v2024b). `https://doi.org/10.5281/zenodo.11394406`

Holland DM and Jenkins A (1999) Modeling thermodynamic ice–ocean interactions at the base of an ice shelf. *Journal of physical oceanography*, **29**(8), 1787–1800

Joughin I, Shapero D and Dutrieux P (2024) Responses of the Pine Island and Thwaites glaciers to melt and sliding parameterizations. *The Cryosphere*, **18**(5), 2583–2601

MacAyeal DR (1989) Large-scale ice flow over a viscous basal sediment: Theory and application to ice stream B, Antarctica. *Journal of Geophysical Research: Solid Earth*, **94**(B4), 4071–4087

McCormack F, Cook S, Phillips S, Adusumilli S, Hattermann T, Nakayama Y, Nias I, Seroussi H, Slater D, Begeman C and others (2023) Ice-ocean melt: Future research directions

Morlighem M, Rignot E, Binder T, Blankenship D, Drews R, Eagles G, Eisen O, Ferraccioli F, Forsberg R, Fretwell P and others (2020) Deep glacial troughs and stabilizing ridges unveiled beneath the margins of the Antarctic ice sheet. *Nature geoscience*, **13**(2), 132–137

Morlighem M, Goldberg D, Barnes JM, Bassis JN, Benn DI, Crawford AJ, Gudmundsson GH and Seroussi H (2024) The West Antarctic Ice Sheet may not be vulnerable to marine ice cliff instability during the 21st century. *Science Advances*, **10**(34), eado7794

Mouginot J, Scheuchl B and Rignot E (2017) MEaSUREs Antarctic Boundaries for IPY 2007-2009 from Satellite Radar, Version 2 (doi: 10.5067/AXE4121732AD)

Nakayama Y, Menemenlis D, Schodlok M and Rignot E (2017) Amundsen and Bellingshausen Seas simulation with optimized ocean, sea ice, and thermodynamic ice shelf model parameters. *Journal of Geophysical Research: Oceans*, **122**(8), 6180–6195

Naughten KA, Meissner KJ, Galton-Fenzi BK, England MH, Timmermann R, Hellmer HH, Hattermann T and Debernard JB (2018) Intercomparison of Antarctic ice-shelf, ocean, and sea-ice interactions simulated by MetROMS-iceshelf and FESOM 1.4. *Geoscientific Model Development*, **11**(4), 1257–1292

Paolo FS, Gardner AS, Greene CA, Nilsson J, Schodlok MP, Schlegel NJ and Fricker HA (2023) Widespread slowdown in thinning rates of west antarctic ice shelves. *The Cryosphere*, **17**(8), 3409–3433

Pearson K (1895) VII. Note on regression and inheritance in the case of two parents. *Proceedings of the Royal Society of London*, **58**(347-352), 240–242

Pelletier C, Fichefet T, Goosse H, Haubner K, Helsen S, Huot PV, Kittel C, Klein F, Le Clec'H S, van Lipzig NP and others (2022) PARASO, a circum-Antarctic fully coupled ice-sheet-ocean-sea-ice-atmosphere-land model involving f.ETISh1.7, NEMO3.6, LIM3.6, COSMO5.0 and CLM4.5. *Geosci. Model Dev.*, **15**, 553–594

Richter O, Timmermann R, Gudmundsson GH and De Rydt J (2025) Coupling framework (1.0) for the Úa (2023b) ice sheet model and the FESOM-1.4 z-coordinate ocean model in an Antarctic domain. *Geoscientific Model Development*, **18**(10), 2945–2960 (doi: https://doi.org/10.5194/gmd-18-2945-2025)

Schaffer J, Timmermann R, Arndt JE, Kristensen SS, Mayer C, Morlighem M and Steinhage D (2016) A global, high-resolution data set of ice sheet topography, cavity geometry, and ocean bathymetry. *Earth System Science Data*, **8**(2), 543–557

Schourup-Kristensen V, Wekerle C, Wolf-Gladrow DA and Völker C (2018) Arctic Ocean biogeochemistry in the high resolution FESOM 1.4-REcoM2 model. *Progress in Oceanography*, **168**, 65–81

Semmler T, Danilov S, Gierz P, Goessling HF, Hegewald J, Hinrichs C, Koldunov N, Khosravi N, Mu L, Rackow T and others (2020) Simulations for CMIP6 with the AWI climate model AWI-CM-1-1. *Journal of Advances in Modeling Earth Systems*, **12**(9), e2019MS002009

Seroussi H, Pelle T, Lipscomb WH, Abe-Ouchi A, Albrecht T, Alvarez-Solas J, Asay-Davis X, Barre JB, Berends CJ, Bernales J and others (2024) Evolution of the Antarctic Ice Sheet over the next three centuries from an ISMIP6 model ensemble. *Earth's Future*, **12**(9), e2024EF004561

Shepherd A, Wingham D and Rignot E (2004) Warm ocean is eroding West Antarctic ice sheet. *Geophysical Research Letters*, **31**(23)

Siahaan A, Smith RS, Holland PR, Jenkins A, Gregory JM, Lee V, Mathiot P, Payne AJ, Ridley JK and Jones CG (2022) The Antarctic contribution to 21st-century sea-level rise predicted by the UK Earth System Model with an interactive ice sheet. *Cryosphere*, **16**(10), 4053–4086

Smith RS, Mathiot P, Siahaan A, Lee V, Cornford SL, Gregory JM, Payne AJ, Jenkins A, Holland PR, Ridley JK and others (2021) Coupling the UK Earth System Model to dynamic models of the Greenland and Antarctic ice sheets. *J. Adv. Model. Earth Sy.*, **13**(10), e2021MS002520

Sun S and Gudmundsson GH (2026) The potential of Marine Ice Cliff Instability for Amundsen Sea glaciers revisited. *Annals of Glaciology*, 1–30 (doi: 10.1017/aog.2026.10046)

Swinscow TDV, Campbell MJ and others (2002) *Statistics at square one*. Ed. 10, Bmj London

Timmermann R and Goeller S (2017) Response to Filchner–Ronne Ice Shelf cavity warming in a coupled ocean–ice sheet model–Part 1: The ocean perspective. *Ocean Science*, **13**(5), 765–776

Timmermann R, Wang Q and Hellmer H (2012) Ice-shelf basal melting in a global finite-element sea-ice/ice-shelf/ocean model. *Annals of Glaciology*, **53**(60), 303–314

Van Wessem JM, Van De Berg WJ, Noël BP, Van Meijgaard E, Amory C, Birnbaum G, Jakobs CL, Krüger K, Lenaerts J, Lhermitte S and others (2018) Modelling the climate and surface mass balance of polar ice sheets using RACMO2–Part 2: Antarctica (1979–2016). *The Cryosphere*, **12**(4), 1479–1498

Walker R, Dupont T, Parizek B and Alley R (2008) Effects of basal-melting distribution on the retreat of ice-shelf grounding lines. *Geophysical Research Letters*, **35**(17)

Wang Q, Danilov S, Sidorenko D, Timmermann R, Wekerle C, Wang X, Jung T and Schröter J (2014) The Finite Element Sea Ice-Ocean Model (FESOM) v. 1.4: formulation of an ocean general circulation model. *Geoscientific Model Development*, **7**(2), 663–693

# APPENDIX: CORRELATION TABLES

| Ice Shelf | Number of elements used in calculation | | | FESOM correlation $C_d = 1.25 \times 10^{-2}$ | | | FESOM correlation $C_d = 2.5 \times 10^{-2}$ | | | Correlation with depth-based melt rate | | |
|---|---|---|---|---|---|---|---|---|---|---|---|---|
| | Adu | Dav | Pao | Adu | Dav | Pao | Adu | Dav | Pao | Adu | Dav | Pao |
| Larsen B | 1102 | 1015 | 960 | 0.23 | -0.13 | **0.40** | 0.11 | -0.22 | **0.66** | 0.39 | 0.14 | **-0.58** |
| Larsen C | 14014 | 13180 | 12935 | 0.10 | 0.22 | 0.25 | 0.08 | 0.21 | 0.37 | 0.03 | 0.28 | 0.16 |
| Larsen D | 6587 | 8147 | 7909 | 0.22 | 0.07 | -0.01 | 0.15 | 0.02 | 0.14 | 0.08 | 0.23 | -0.04 |
| Ronne | 80885 | 74443 | 71513 | **0.44** | **0.46** | 0.34 | **0.54** | **0.57** | **0.46** | -0.13 | -0.14 | -0.16 |
| Filchner | 31494 | 29072 | 27611 | 0.35 | **0.51** | **0.44** | 0.37 | **0.53** | **0.53** | -0.10 | 0.12 | 0.10 |
| Brunt | 8705 | 9063 | 8569 | **0.42** | 0.24 | 0.13 | **0.43** | **0.40** | 0.14 | 0.21 | 0.13 | 0.03 |
| Riiser-Larsen | 13222 | 12745 | 12017 | 0.10 | 0.17 | 0.29 | 0.27 | 0.31 | 0.33 | 0.02 | 0.12 | 0.30 |
| Quar | 1168 | 1112 | 966 | -0.10 | -0.10 | 0.02 | 0.26 | 0.20 | -0.28 | -0.07 | -0.16 | -0.11 |
| Ekstrom | 3159 | 3082 | 2737 | -0.03 | -0.17 | 0.12 | 0.26 | 0.29 | 0.09 | -0.10 | -0.22 | 0.22 |
| Atka | 874 | 838 | 740 | 0.10 | -0.06 | -0.35 | 0.28 | **0.43** | **0.70** | 0.29 | 0.07 | -0.14 |
| Jelbart | 4506 | 4320 | 4006 | 0.38 | **0.43** | 0.37 | **0.45** | **0.45** | 0.36 | 0.01 | 0.10 | 0.15 |
| Fimbul | 11170 | 10495 | 9966 | **0.56** | **0.58** | 0.35 | **0.68** | **0.67** | **0.47** | 0.14 | 0.24 | 0.10 |
| Vigrid | 1097 | 1071 | 923 | **-0.43** | -0.24 | -0.37 | 0.10 | **0.41** | 0.37 | **-0.57** | **-0.50** | **-0.59** |
| Nivl | 3016 | 2897 | 2623 | -0.20 | -0.04 | -0.24 | **0.49** | **0.40** | **0.50** | -0.30 | -0.13 | -0.38 |
| Lazarev | 2692 | 2499 | 2396 | -0.15 | 0.18 | 0.15 | 0.36 | 0.23 | 0.03 | -0.17 | 0.13 | 0.13 |
| Borchgrevink | 8185 | 7911 | 7497 | -0.12 | 0.12 | 0.04 | -0.02 | 0.23 | 0.16 | -0.31 | -0.10 | -0.03 |
| Baudouin | 9587 | 9066 | 8839 | 0.26 | **0.43** | **0.52** | 0.32 | **0.48** | **0.53** | -0.07 | 0.06 | 0.27 |
| Prince Harald | 2074 | 2191 | 1903 | 0.09 | 0.32 | **0.55** | 0.21 | **0.45** | **0.62** | 0.06 | 0.17 | **0.51** |
| Amery | 21026 | 20133 | 18172 | **0.64** | **0.68** | **0.58** | **0.67** | **0.70** | **0.62** | 0.08 | 0.21 | 0.22 |
| West | 5607 | 5025 | 4842 | 0.05 | 0.06 | -0.10 | 0.02 | 0.03 | -0.02 | 0.06 | -0.02 | -0.10 |
| Shackleton | 6339 | 5790 | 5577 | 0.28 | 0.20 | 0.21 | 0.08 | 0.03 | 0.06 | -0.04 | 0.04 | 0.20 |
| Tracy Tremenchus | 0 | 1047 | 983 | | **0.43** | **0.40** | | **0.47** | 0.33 | | 0.11 | 0.30 |
| Conger-Glenzer | 0 | 569 | 558 | | 0.01 | -0.10 | | 0.06 | **0.59** | | -0.13 | -0.13 |
| Totten | 2920 | 2800 | 2184 | 0.06 | 0.20 | 0.02 | 0.02 | 0.16 | 0.29 | 0.05 | 0.19 | -0.19 |
| Moscow University | 2825 | 2750 | 2361 | 0.23 | **0.55** | **0.49** | 0.32 | **0.59** | **0.61** | 0.04 | 0.09 | 0.18 |
| Holmes | 932 | 964 | 871 | 0.22 | **0.51** | **0.42** | 0.11 | 0.27 | -0.10 | 0.08 | 0.18 | 0.05 |
| Dibble | 0 | 715 | 554 | | **0.49** | 0.30 | | **0.53** | 0.29 | | -0.11 | -0.33 |
| Mertz | 1567 | 1313 | 1405 | **0.53** | **0.54** | -0.28 | **0.58** | **0.60** | -0.15 | 0.35 | **0.42** | **-0.40** |
| Ninnis | 0 | 451 | 662 | | **0.58** | 0.36 | | **0.50** | 0.38 | | -0.20 | 0.38 |
| Cook | 1542 | 1476 | 1292 | 0.18 | 0.00 | 0.07 | 0.08 | -0.09 | 0.08 | 0.22 | -0.19 | 0.10 |
| Rennick | 1729 | 1702 | 1625 | -0.01 | -0.13 | -0.02 | -0.01 | -0.14 | -0.11 | 0.30 | 0.22 | 0.25 |
| Lillie | 0 | 303 | 287 | | 0.16 | 0.14 | | 0.09 | 0.03 | | -0.34 | -0.16 |

| | | | | | | | | | | | |
|---|---|---|---|---|---|---|---|---|---|---|---|
| Mariner | 1215 | 988 | 1061 | -0.10 | 0.03 | 0.32 | -0.06 | -0.13 | 0.37 | 0.21 | -0.01 | -0.29 |
| Nansen | 924 | 772 | 731 | 0.13 | -0.24 | **-0.41** | 0.20 | -0.04 | **-0.47** | -0.15 | 0.20 | 0.37 |
| Drygalski | 479 | 521 | 656 | -0.13 | -0.22 | 0.19 | 0.02 | -0.16 | -0.12 | **0.42** | -0.30 | -0.30 |
| Ross East | 33357 | 32189 | 29963 | 0.29 | 0.31 | 0.28 | 0.29 | **0.40** | **0.41** | 0.03 | -0.04 | -0.05 |
| Ross West | 50143 | 46342 | 44035 | 0.16 | 0.06 | 0.13 | 0.23 | 0.27 | 0.09 | 0.14 | -0.13 | 0.14 |
| Sulzberger | 4949 | 4440 | 3947 | **0.40** | 0.38 | **0.53** | **0.40** | 0.39 | **0.54** | 0.36 | 0.36 | **0.49** |
| Nickerson | 2679 | 2724 | 2336 | 0.27 | **0.46** | **0.45** | 0.31 | **0.43** | 0.19 | 0.18 | 0.23 | **0.43** |
| Getz | 14664 | 13629 | 12925 | 0.15 | 0.18 | 0.13 | 0.09 | 0.13 | 0.12 | 0.10 | 0.23 | 0.22 |
| Dotson | 2724 | 2712 | 2043 | **0.45** | **0.61** | **0.52** | 0.24 | **0.42** | 0.27 | 0.22 | 0.30 | 0.33 |
| Crosson | 1279 | 1015 | 1246 | **0.42** | **0.69** | **0.82** | **0.41** | **0.59** | **0.81** | **0.50** | **0.43** | **0.83** |
| Thwaites | 971 | 505 | 1050 | 0.01 | **0.43** | 0.31 | -0.20 | 0.14 | 0.21 | -0.16 | 0.26 | 0.23 |
| Pine Island | 2964 | 2248 | 2493 | **0.62** | **0.77** | **0.49** | **0.48** | **0.61** | 0.33 | **0.49** | **0.50** | **0.40** |
| Cosgrove | 1689 | 1486 | 1402 | 0.27 | 0.28 | 0.22 | 0.12 | 0.13 | 0.11 | 0.13 | 0.10 | 0.17 |
| Abbot | 10871 | 10352 | 9473 | 0.27 | **0.49** | **0.54** | **0.41** | **0.52** | **0.64** | 0.24 | 0.39 | **0.45** |
| Venable | 1562 | 1482 | 1370 | 0.07 | 0.15 | -0.09 | 0.06 | 0.14 | 0.01 | 0.07 | 0.06 | 0.01 |
| Stange | 3641 | 3513 | 3216 | **0.50** | **0.57** | **0.55** | **0.66** | **0.69** | **0.72** | **0.52** | **0.57** | **0.56** |
| George VI | 11358 | 10549 | 10029 | 0.19 | 0.19 | 0.20 | 0.24 | 0.22 | 0.27 | 0.12 | 0.16 | 0.20 |
| Bach | 2662 | 2393 | 2118 | -0.03 | -0.12 | -0.24 | -0.02 | -0.12 | -0.23 | 0.05 | 0.13 | 0.16 |
| Wilkins | 4506 | 3943 | 3909 | 0.00 | 0.06 | 0.03 | 0.00 | 0.07 | 0.05 | 0.27 | **0.48** | **0.40** |

**Table 4.** This table details correlations between melt rates on each of our chosen ice shelves, calculated on Ice Mesh 1. The first columns show the number of elements included in calculations with each observationally-derived dataset. Differences in coverage mean these are not all the same. An area-weighted Pearson's Correlation Coefficient was calculated between the observationally-derived datasets and outputs from FESOM - using two different values for turbulent exchange coefficient $C_d$ - as well as a simple depth-dependent melt rate. Ice shelves are listed by position, clockwise around Antarctica starting at the tip of the Peninsula. The strength of coloured shading indicates the strength of similarity, with red for positive and blue for negative correlation. Values in bold have magnitude $\geqslant 0.4$ and are counted as a moderate correlation, while values in a coloured font have magnitude $\geqslant 0.6$ and are counted as a strong correlation. We refer to the datasets by abbreviations of the first author names; Adu for Adusumilli and others (2020), Dav for Davison and others (2023) and Pao for Paolo and others (2023).

| Ice Shelf | Number of elements used in correlation | | | | Correlation between dataset pairs | | | |
|---|---|---|---|---|---|---|---|---|
| | FESOM | Adu-Dav | Adu-Pao | Dav-Pao | FESOM | Adu-Dav | Adu-Pao | Dav-Pao |
| Larsen B | 1350 | 992 | 929 | 886 | **0.78** | **0.41** | -0.22 | -0.21 |
| Larsen C | 15954 | 13130 | 12455 | 12254 | **0.79** | **0.41** | 0.07 | 0.31 |
| Larsen D | 11344 | 5429 | 5415 | 7237 | **0.78** | 0.28 | 0.11 | 0.07 |
| Ronne | 83094 | 74402 | 71458 | 70676 | **0.84** | **0.71** | **0.61** | **0.72** |

| | | | | | | | | |
|---|---|---|---|---|---|---|---|---|
| Filchner | 32205 | 28977 | 27550 | 27420 | **0.84** | **0.46** | 0.37 | **0.67** |
| Brunt | 10181 | 8253 | 8028 | 8281 | 0.33 | **0.63** | 0.21 | 0.23 |
| Riiser-Larsen | 14295 | 12605 | 11900 | 11833 | -0.14 | **0.55** | **0.50** | **0.63** |
| Quar | 1329 | 1105 | 965 | 959 | -0.34 | 0.19 | 0.10 | 0.29 |
| Ekstrom | 3501 | 3039 | 2729 | 2725 | -0.34 | **0.46** | 0.30 | **0.40** |
| Atka | 981 | 830 | 738 | 732 | **-0.46** | 0.30 | 0.25 | **0.41** |
| Jelbart | 5065 | 4295 | 3982 | 3987 | **0.91** | **0.40** | 0.29 | **0.47** |
| Fimbul | 12281 | 10439 | 9903 | 9734 | **0.90** | **0.67** | **0.59** | **0.65** |
| Vigrid | 1267 | 1048 | 917 | 922 | 0.29 | **0.46** | **0.44** | **0.70** |
| Nivl | 3365 | 2854 | 2612 | 2567 | 0.11 | **0.58** | **0.61** | **0.60** |
| Lazarev | 2958 | 2481 | 2376 | 2300 | -0.24 | **0.48** | 0.13 | **0.47** |
| Borchgrevink | 9181 | 7738 | 7304 | 7303 | **0.95** | **0.51** | 0.32 | **0.48** |
| Baudouin | 10342 | 9047 | 8771 | 8634 | **0.90** | **0.74** | 0.28 | **0.57** |
| Prince Harald | 2846 | 1870 | 1685 | 1792 | **0.86** | **0.46** | 0.22 | **0.53** |
| Amery | 22989 | 19805 | 18120 | 17850 | **0.97** | **0.75** | **0.72** | **0.77** |
| West | 6503 | 4935 | 4750 | 4480 | -0.09 | 0.31 | 0.05 | 0.36 |
| Shackleton | 7299 | 5647 | 5442 | 5239 | **0.41** | 0.39 | 0.18 | **0.41** |
| Tracy Tremenchus | 1534 | 0 | 0 | 880 | **0.92** | | | 0.38 |
| Conger-Glenzer | 714 | 0 | 0 | 511 | -0.19 | | | 0.37 |
| Totten | 3600 | 2624 | 2145 | 2033 | **0.80** | **0.64** | **0.41** | **0.74** |
| Moscow University | 3792 | 2584 | 2250 | 2293 | **0.57** | 0.31 | 0.39 | **0.71** |
| Holmes | 1483 | 749 | 712 | 801 | 0.10 | 0.37 | -0.05 | **0.49** |
| Dibble | 888 | 0 | 0 | 548 | **0.94** | | | **0.75** |
| Mertz | 1795 | 1295 | 1378 | 1231 | **0.97** | **0.48** | -0.06 | 0.18 |
| Ninnis | 1167 | 0 | 0 | 343 | **0.86** | | | 0.29 |
| Cook | 1785 | 1444 | 1292 | 1280 | **0.86** | -0.23 | -0.01 | 0.18 |
| Rennick | 2232 | 1537 | 1486 | 1539 | **0.81** | 0.36 | **0.41** | **0.84** |
| Lillie | 550 | 0 | 0 | 231 | **0.94** | | | **0.48** |
| Mariner | 1603 | 962 | 1011 | 882 | 0.23 | 0.30 | 0.25 | 0.11 |
| Nansen | 1252 | 748 | 714 | 637 | **0.86** | 0.04 | -0.17 | 0.03 |
| Drygalski | 1011 | 367 | 389 | 454 | **0.71** | 0.01 | -0.17 | **0.56** |
| Ross East | 36300 | 31194 | 29159 | 29743 | **0.52** | **0.55** | **0.54** | **0.52** |
| Ross West | 51215 | 46297 | 43941 | 43478 | 0.19 | **0.44** | 0.10 | 0.21 |
| Sulzberger | 6884 | 4287 | 3764 | 3695 | **0.98** | **0.80** | **0.77** | **0.85** |
| Nickerson | 3411 | 2494 | 2206 | 2286 | **0.78** | **0.64** | **0.45** | **0.52** |
| Getz | 16613 | 13544 | 12766 | 12447 | **0.82** | **0.56** | **0.42** | **0.65** |
| Dotson | 3521 | 2486 | 2033 | 2004 | **0.92** | **0.70** | **0.70** | **0.86** |

| | | | | | | | | |
|---|---|---|---|---|---|---|---|---|
| Crosson | 1938 | 691 | 1040 | 725 | **0.98** | **0.55** | **0.54** | **0.69** |
| Thwaites | 1729 | 415 | 738 | 295 | **0.93** | **0.82** | 0.17 | -0.04 |
| Pine Island | 3672 | 2027 | 2383 | 1837 | **0.92** | **0.78** | **0.62** | **0.87** |
| Cosgrove | 2015 | 1456 | 1396 | 1312 | **0.94** | **0.50** | **0.41** | **0.68** |
| Abbot | 13377 | 9898 | 9137 | 8919 | **0.87** | **0.53** | **0.57** | **0.82** |
| Venable | 1830 | 1444 | 1354 | 1332 | **0.88** | **0.41** | 0.24 | 0.12 |
| Stange | 4586 | 3253 | 3076 | 3068 | **0.91** | **0.82** | **0.82** | **0.86** |
| George VI | 13051 | 10437 | 9838 | 9612 | **0.92** | **0.64** | **0.54** | **0.71** |
| Bach | 3185 | 2365 | 2102 | 2008 | **0.98** | 0.35 | 0.22 | **0.52** |
| Wilkins | 5572 | 3860 | 3747 | 3428 | **0.92** | **0.71** | **0.54** | **0.78** |

**Table 5.** Correlation coefficients between the two different FESOM outputs, and each pair of observational datasets. The ice sheet model mesh, Ice Mesh 1, is the same as in Table 6.

| Ice Shelf | Number of elements used in calculation | | | FESOM correlation $C_d = 1.25 \times 10^{-2}$ | | | FESOM correlation $C_d = 2.5 \times 10^{-2}$ | | | Correlation with depth-based melt rate | | |
|---|---|---|---|---|---|---|---|---|---|---|---|---|
| | Adu | Dav | Pao | Adu | Dav | Pao | Adu | Dav | Pao | Adu | Dav | Pao |
| Larsen B | 1575 | 1478 | 1421 | 0.18 | -0.26 | 0.38 | 0.11 | -0.24 | **0.66** | 0.38 | 0.13 | **-0.59** |
| Larsen C | 29528 | 28508 | 29979 | 0.09 | 0.22 | 0.24 | 0.07 | 0.20 | 0.36 | 0.07 | 0.28 | 0.21 |
| Larsen D | 11084 | 14362 | 13759 | 0.21 | 0.07 | -0.02 | 0.14 | 0.01 | 0.13 | 0.08 | 0.24 | -0.03 |
| Ronne | 201894 | 193548 | 189765 | **0.41** | **0.45** | 0.34 | **0.52** | **0.56** | **0.47** | -0.13 | -0.13 | -0.15 |
| Filchner | 71979 | 68820 | 66935 | 0.33 | **0.51** | **0.44** | 0.35 | **0.53** | **0.53** | -0.10 | 0.14 | 0.12 |
| Brunt | 22047 | 22778 | 22281 | 0.36 | 0.18 | 0.13 | 0.38 | 0.35 | 0.14 | 0.22 | 0.14 | 0.02 |
| Riiser-Larsen | 30089 | 29232 | 28170 | 0.10 | 0.17 | 0.29 | 0.26 | 0.30 | 0.33 | 0.04 | 0.15 | 0.32 |
| Quar | 1732 | 1664 | 1465 | -0.11 | -0.11 | 0.05 | 0.25 | 0.20 | -0.27 | -0.05 | -0.15 | -0.11 |
| Ekstrom | 5490 | 5440 | 4925 | -0.05 | -0.20 | 0.11 | 0.25 | 0.29 | 0.08 | -0.08 | -0.21 | 0.23 |
| Atka | 1446 | 1409 | 1270 | 0.12 | -0.06 | -0.35 | 0.31 | **0.42** | **0.70** | 0.32 | 0.09 | -0.13 |
| Jelbart | 8313 | 8093 | 7625 | **0.40** | **0.43** | 0.38 | **0.47** | **0.46** | 0.38 | 0.02 | 0.09 | 0.14 |
| Fimbul | 26038 | 24431 | 24020 | **0.49** | **0.55** | 0.36 | **0.60** | **0.65** | **0.49** | 0.16 | 0.28 | 0.14 |
| Vigrid | 1700 | 1676 | 1493 | **-0.41** | -0.25 | -0.39 | 0.11 | **0.42** | 0.38 | **-0.57** | **-0.49** | **-0.56** |
| Nivl | 5582 | 5415 | 5038 | -0.18 | -0.03 | -0.23 | **0.49** | 0.39 | **0.51** | -0.30 | -0.10 | -0.35 |
| Lazarev | 5954 | 5586 | 5446 | -0.16 | 0.18 | 0.16 | 0.37 | 0.21 | 0.05 | -0.16 | 0.14 | 0.11 |
| Borchgrevink | 15665 | 15242 | 14698 | -0.14 | 0.08 | 0.05 | -0.04 | 0.20 | 0.17 | -0.32 | -0.09 | -0.02 |
| Baudouin | 22533 | 21606 | 21406 | 0.20 | 0.39 | **0.53** | 0.27 | **0.44** | **0.54** | -0.06 | 0.09 | 0.27 |
| Prince Harald | 3244 | 3439 | 3042 | 0.13 | 0.31 | **0.56** | 0.26 | **0.44** | **0.63** | 0.15 | 0.20 | **0.54** |
| Amery | 43778 | 42297 | 40030 | **0.63** | **0.68** | **0.58** | **0.67** | **0.71** | **0.63** | 0.09 | 0.22 | 0.22 |
| West | 10756 | 9521 | 9548 | 0.00 | 0.04 | -0.09 | 0.01 | 0.02 | -0.01 | 0.07 | -0.01 | -0.11 |

| | | | | | | | | | | | | |
|---|---|---|---|---|---|---|---|---|---|---|---|---|
| Shackleton | 15555 | 14262 | 14370 | 0.06 | 0.07 | 0.20 | 0.00 | -0.02 | 0.06 | -0.05 | 0.04 | 0.20 |
| Tracy Tremenchus | 0 | 1781 | 1699 | | **0.40** | **0.41** | | **0.44** | 0.38 | | 0.24 | 0.21 |
| Conger-Glenzer | 0 | 991 | 956 | | 0.01 | -0.08 | | 0.07 | **0.60** | | -0.14 | -0.12 |
| Totten | 4564 | 4301 | 3542 | 0.04 | 0.21 | 0.01 | 0.00 | 0.17 | 0.29 | 0.03 | 0.16 | -0.19 |
| Moscow University | 4188 | 4093 | 3637 | 0.22 | **0.51** | **0.50** | 0.31 | **0.55** | **0.62** | 0.03 | 0.15 | 0.20 |
| Holmes | 1338 | 1371 | 1233 | 0.14 | **0.40** | **0.43** | 0.02 | 0.11 | -0.10 | 0.18 | 0.19 | 0.03 |
| Dibble | 0 | 1094 | 849 | | 0.38 | 0.14 | | 0.39 | 0.09 | | -0.11 | -0.34 |
| Mertz | 2597 | 2123 | 2381 | **0.49** | **0.52** | -0.28 | **0.55** | **0.59** | -0.15 | 0.34 | **0.42** | **-0.41** |
| Ninnis | 0 | 611 | 941 | | 0.27 | 0.35 | | 0.30 | 0.37 | | -0.16 | 0.36 |
| Cook | 2601 | 2540 | 2215 | 0.16 | -0.01 | 0.08 | 0.08 | -0.09 | 0.08 | 0.19 | -0.17 | 0.13 |
| Rennick | 2387 | 2373 | 2288 | -0.05 | -0.18 | -0.06 | -0.03 | -0.16 | -0.12 | 0.32 | 0.24 | 0.27 |
| Lillie | 0 | 382 | 372 | | 0.17 | 0.11 | | 0.10 | -0.01 | | -0.36 | -0.26 |
| Mariner | 1726 | 1426 | 1528 | -0.11 | 0.02 | 0.31 | -0.07 | -0.14 | 0.38 | 0.25 | 0.04 | -0.28 |
| Nansen | 1319 | 1100 | 1086 | 0.13 | -0.18 | -0.38 | 0.25 | -0.03 | **-0.47** | -0.16 | 0.24 | 0.38 |
| Drygalski | 1070 | 1014 | 1257 | -0.14 | -0.22 | -0.15 | 0.02 | -0.14 | -0.27 | **0.46** | -0.35 | -0.28 |
| Ross East | 94548 | 93422 | 90679 | 0.29 | 0.30 | 0.29 | 0.29 | **0.40** | **0.43** | 0.04 | -0.03 | -0.03 |
| Ross West | 147401 | 142105 | 138413 | 0.16 | 0.05 | 0.13 | 0.23 | 0.27 | 0.10 | 0.14 | -0.12 | 0.15 |
| Sulzberger | 7418 | 6790 | 6145 | **0.40** | 0.36 | **0.54** | **0.40** | 0.37 | **0.54** | **0.40** | 0.36 | **0.50** |
| Nickerson | 4294 | 4433 | 3879 | 0.24 | 0.36 | **0.43** | 0.26 | 0.27 | 0.15 | 0.20 | 0.24 | **0.42** |
| Getz | 25186 | 23656 | 22845 | 0.13 | 0.18 | 0.13 | 0.07 | 0.12 | 0.12 | 0.10 | 0.24 | 0.25 |
| Dotson | 4243 | 4202 | 3314 | **0.45** | **0.63** | **0.54** | 0.23 | **0.44** | 0.28 | 0.29 | 0.36 | 0.34 |
| Crosson | 1950 | 1490 | 1961 | **0.43** | **0.70** | **0.84** | **0.42** | **0.61** | **0.83** | **0.50** | **0.44** | **0.83** |
| Thwaites | 1776 | 808 | 1968 | 0.01 | **0.42** | 0.31 | -0.22 | 0.11 | 0.21 | -0.18 | 0.25 | 0.25 |
| Pine Island | 4546 | 3316 | 3941 | **0.62** | **0.77** | **0.50** | **0.48** | **0.62** | 0.34 | **0.51** | **0.51** | **0.41** |
| Cosgrove | 2418 | 2143 | 2081 | 0.23 | 0.23 | 0.18 | 0.08 | 0.08 | 0.07 | 0.14 | 0.21 | 0.13 |
| Abbot | 20048 | 19462 | 18127 | 0.26 | **0.47** | **0.54** | **0.41** | **0.51** | **0.64** | 0.28 | **0.40** | **0.47** |
| Venable | 2415 | 2315 | 2152 | 0.02 | 0.09 | -0.09 | 0.01 | 0.08 | 0.01 | 0.06 | 0.03 | 0.00 |
| Stange | 5720 | 5591 | 5269 | **0.51** | **0.58** | **0.55** | **0.67** | **0.70** | **0.73** | **0.54** | **0.59** | **0.57** |
| George VI | 18300 | 17134 | 16690 | 0.19 | 0.17 | 0.21 | 0.24 | 0.20 | 0.28 | 0.13 | 0.17 | 0.20 |
| Bach | 3661 | 3324 | 3009 | -0.04 | -0.15 | -0.26 | -0.03 | -0.15 | -0.25 | 0.03 | 0.16 | 0.11 |
| Wilkins | 7620 | 6823 | 7010 | -0.02 | 0.04 | 0.02 | -0.03 | 0.06 | 0.04 | 0.30 | **0.50** | **0.41** |

**Table 6.** Exactly as Table 4, for calculations on Ice Mesh 2.

| Ice Shelf | FESOM correlation $C_d = 1.25 \times 10^{-2}$ 5 km gridded data | FESOM correlation $C_d = 2.5 \times 10^{-2}$ 5 km gridded data | FESOM correlation $C_d = 1.25 \times 10^{-2}$ 20 km gridded data | FESOM correlation $C_d = 2.5 \times 10^{-2}$ 20 km gridded data |
|---|---|---|---|---|

| | Adu | Dav | Pao | Adu | Dav | Pao | Adu | Dav | Pao | Adu | Dav | Pao |
|---|---|---|---|---|---|---|---|---|---|---|---|---|
| Larsen B | 0.18 | -0.26 | **0.43** | 0.10 | -0.26 | **0.70** | -0.12 | **-0.51** | **0.68** | -0.03 | -0.36 | **0.70** |
| Larsen C | 0.10 | 0.22 | 0.25 | 0.07 | 0.20 | 0.37 | 0.14 | 0.25 | 0.25 | 0.09 | 0.23 | 0.36 |
| Larsen D | 0.21 | 0.06 | -0.01 | 0.14 | 0.00 | 0.14 | 0.23 | 0.06 | 0.05 | 0.18 | 0.03 | 0.18 |
| Ronne | **0.42** | **0.46** | 0.35 | **0.53** | **0.57** | **0.48** | 0.39 | **0.43** | 0.31 | **0.52** | **0.57** | **0.47** |
| Filchner | 0.33 | **0.52** | **0.45** | 0.35 | **0.53** | **0.54** | 0.32 | **0.52** | **0.46** | 0.35 | **0.52** | **0.55** |
| Brunt | 0.36 | 0.19 | 0.13 | 0.39 | 0.36 | 0.14 | 0.39 | 0.23 | 0.17 | 0.38 | 0.38 | 0.16 |
| Riiser-Larsen | 0.10 | 0.17 | 0.30 | 0.26 | 0.30 | 0.33 | 0.08 | 0.14 | 0.24 | 0.25 | 0.28 | 0.31 |
| Quar | -0.09 | -0.11 | 0.02 | 0.26 | 0.21 | -0.27 | 0.02 | -0.07 | 0.16 | 0.27 | 0.30 | -0.11 |
| Ekstrom | -0.07 | -0.21 | 0.12 | 0.25 | 0.29 | 0.08 | -0.12 | -0.29 | 0.11 | 0.19 | 0.25 | 0.06 |
| Atka | 0.13 | -0.07 | -0.36 | 0.30 | **0.41** | **0.71** | -0.02 | -0.04 | -0.29 | 0.18 | 0.29 | **0.65** |
| Jelbart | **0.40** | **0.46** | 0.39 | **0.48** | **0.48** | 0.39 | 0.34 | **0.50** | **0.41** | **0.45** | **0.53** | **0.43** |
| Fimbul | **0.48** | **0.56** | 0.37 | **0.60** | **0.66** | **0.49** | **0.48** | **0.56** | 0.39 | **0.65** | **0.70** | **0.56** |
| Vigrid | **-0.45** | -0.30 | **-0.40** | 0.16 | **0.45** | **0.45** | **-0.56** | -0.27 | **-0.40** | **0.40** | **0.49** | **0.44** |
| Nivl | -0.19 | -0.02 | -0.23 | **0.51** | **0.40** | **0.53** | -0.20 | 0.03 | -0.18 | **0.57** | **0.45** | **0.64** |
| Lazarev | -0.15 | 0.19 | 0.18 | 0.37 | 0.21 | 0.06 | -0.17 | 0.19 | 0.15 | 0.37 | 0.23 | 0.12 |
| Borchgrevink | -0.16 | 0.08 | 0.05 | -0.05 | 0.20 | 0.17 | -0.17 | 0.07 | 0.06 | -0.06 | 0.18 | 0.16 |
| Baudouin | 0.20 | 0.39 | **0.54** | 0.27 | **0.45** | **0.55** | 0.12 | 0.27 | **0.47** | 0.20 | 0.34 | **0.50** |
| Prince Harald | 0.14 | 0.31 | **0.58** | 0.27 | **0.44** | **0.65** | 0.13 | 0.28 | **0.57** | 0.09 | 0.32 | **0.61** |
| Amery | **0.63** | **0.68** | **0.57** | **0.66** | **0.71** | **0.62** | **0.60** | **0.65** | **0.52** | **0.64** | **0.69** | **0.55** |
| West | 0.01 | 0.05 | -0.10 | 0.01 | 0.02 | -0.02 | -0.01 | 0.04 | -0.18 | 0.09 | -0.06 | -0.12 |
| Shackleton | 0.06 | 0.07 | 0.21 | -0.01 | -0.03 | 0.05 | -0.03 | 0.10 | 0.10 | -0.05 | -0.04 | -0.01 |
| Tracy Tremenchus | | **0.40** | **0.41** | | **0.43** | 0.37 | | 0.32 | **0.42** | | 0.35 | 0.35 |
| Conger-Glenzer | | 0.01 | -0.11 | | 0.09 | **0.62** | | 0.32 | **0.49** | | 0.13 | **0.62** |
| Totten | 0.07 | 0.23 | 0.02 | 0.01 | 0.18 | 0.31 | 0.00 | 0.18 | -0.08 | -0.12 | 0.02 | 0.21 |
| Moscow University | 0.24 | **0.56** | **0.55** | 0.33 | **0.58** | **0.66** | 0.31 | **0.61** | **0.58** | 0.23 | **0.49** | **0.46** |
| Holmes | 0.17 | **0.45** | **0.46** | 0.00 | 0.11 | -0.12 | 0.23 | **0.43** | 0.26 | -0.34 | -0.36 | -0.14 |
| Dibble | | **0.45** | 0.29 | | **0.48** | 0.24 | | **0.51** | **0.45** | | **0.58** | **0.46** |
| Mertz | **0.48** | **0.55** | -0.29 | **0.55** | **0.62** | -0.15 | **0.43** | **0.57** | **-0.40** | **0.54** | **0.68** | -0.16 |
| Ninnis | | 0.28 | 0.34 | | 0.29 | 0.37 | | 0.29 | 0.27 | | **0.40** | 0.35 |
| Cook | 0.16 | -0.03 | 0.09 | 0.08 | -0.09 | 0.10 | 0.19 | 0.00 | -0.02 | 0.15 | -0.16 | -0.01 |
| Rennick | -0.08 | -0.19 | -0.08 | -0.04 | -0.15 | -0.13 | -0.33 | -0.30 | -0.28 | -0.11 | -0.11 | -0.22 |
| Lillie | | 0.06 | 0.12 | | -0.02 | 0.00 | | -0.05 | 0.31 | | -0.35 | -0.20 |
| Mariner | -0.10 | 0.01 | 0.34 | -0.10 | -0.14 | 0.37 | -0.08 | -0.04 | **0.46** | -0.10 | -0.13 | **0.55** |
| Nansen | 0.14 | -0.20 | **-0.43** | 0.27 | -0.03 | **-0.51** | 0.07 | -0.13 | **-0.43** | 0.22 | 0.09 | **-0.45** |
| Drygalski | -0.14 | -0.29 | -0.15 | 0.06 | -0.22 | -0.30 | 0.30 | -0.29 | 0.07 | 0.22 | -0.17 | -0.08 |
| Ross East | 0.29 | 0.31 | 0.29 | 0.30 | **0.40** | **0.43** | 0.27 | 0.29 | 0.25 | 0.29 | 0.38 | **0.43** |

| | | | | | | | | | | | | |
|---|---|---|---|---|---|---|---|---|---|---|---|---|
| Ross West | 0.17 | 0.05 | 0.14 | 0.23 | 0.27 | 0.10 | 0.18 | 0.07 | 0.15 | 0.26 | 0.32 | 0.06 |
| Sulzberger | **0.41** | 0.37 | **0.55** | **0.41** | 0.38 | **0.56** | 0.39 | 0.35 | **0.53** | **0.41** | 0.38 | **0.58** |
| Nickerson | 0.23 | 0.36 | **0.43** | 0.26 | 0.27 | 0.13 | 0.10 | 0.29 | **0.49** | 0.09 | 0.17 | 0.18 |
| Getz | 0.15 | 0.20 | 0.15 | 0.09 | 0.13 | 0.14 | 0.18 | 0.31 | 0.24 | 0.08 | 0.16 | 0.18 |
| Dotson | **0.47** | **0.68** | **0.54** | 0.21 | **0.45** | 0.25 | **0.41** | **0.67** | **0.47** | 0.24 | **0.54** | 0.28 |
| Crosson | **0.49** | **0.76** | **0.86** | **0.49** | **0.66** | **0.85** | **0.52** | **0.73** | **0.88** | **0.53** | **0.67** | **0.88** |
| Thwaites | 0.02 | **0.40** | 0.34 | -0.24 | 0.12 | 0.25 | 0.17 | **0.70** | **0.67** | 0.06 | **0.59** | **0.67** |
| Pine Island | **0.64** | **0.78** | **0.50** | **0.49** | **0.60** | 0.33 | **0.40** | **0.77** | **0.51** | 0.24 | **0.63** | 0.36 |
| Cosgrove | 0.26 | 0.25 | 0.22 | 0.09 | 0.09 | 0.10 | 0.17 | 0.23 | 0.06 | -0.03 | 0.04 | -0.07 |
| Abbot | 0.27 | **0.48** | **0.56** | **0.43** | **0.53** | **0.68** | 0.18 | **0.43** | **0.50** | 0.37 | **0.53** | **0.66** |
| Venable | 0.04 | 0.10 | -0.02 | -0.01 | 0.06 | 0.08 | -0.10 | -0.01 | -0.13 | -0.09 | -0.11 | -0.10 |
| Stange | **0.54** | **0.64** | **0.60** | **0.70** | **0.76** | **0.78** | 0.38 | **0.54** | **0.44** | **0.46** | **0.59** | **0.54** |
| George VI | 0.21 | 0.17 | 0.23 | 0.26 | 0.20 | 0.30 | 0.24 | 0.12 | 0.24 | 0.29 | 0.14 | 0.30 |
| Bach | -0.04 | -0.16 | -0.27 | -0.03 | -0.16 | -0.26 | -0.07 | -0.25 | **-0.42** | -0.05 | -0.26 | **-0.41** |
| Wilkins | -0.04 | 0.05 | 0.01 | -0.05 | 0.06 | 0.03 | -0.06 | -0.03 | -0.06 | -0.06 | -0.03 | -0.05 |

**Table 7.** Correlation coefficients using regridded FESOM outputs at two different resolutions: 5 km and 20 km. The ice sheet model mesh, Ice Mesh 2, and therefore the number of elements used for each calculation, is the same as in Table 6.